AD

AD730669

REPORT NO. RD-TR-71-17

ROCKET PLUME EFFECTS ON BOATTAIL AND FLARE BODIES OF REVOLUTION AT TRANSONIC SPEEDS

by

Donald V. Rubin

May 1971

Approved for public release; distribution unlimited.

U.S. ARMY MISSILE COMMAND

Redstone Arsenal, Alabama

DDC

RECEIVED

OCT 12 1971

C

Reproduced by

NATIONAL TECHNICAL INFORMATION SERVICE

Springfield Va. 22151

FORM AMSMI-1021, 1 DEC 65 PREVIOUS EDITION IS OBSOLETE

46

14. KEY WORDS	LINK A ROLE	LINK A WT	LINK B ROLE	LINK B WT	LINK C ROLE	LINK C WT
Boattail Bodies						
Flare Bodies						
Rocket plume effects						
Revolution at transonic speeds						
Jet plume						

ACCESSION for
NTIS WHITE SECTION ☑
DDC BUFF SECTION ☐
UNANNOUNCED ☐
JUSTIFICATION
BY
DISTRIBUTION/AVAILABILITY CODES
DIST. AVAIL. and/or SPECIAL
A

DISPOSITION INSTRUCTIONS

Destroy this report when it is no longer needed. Do not return it to the originator.

DISCLAIMER

The findings in this report are not to be construed as an official Department of the Army position unless so designated by other authorized documents.

TRADE NAMES

Use of trade names or manufacturers in this report does not constitute an official indorsement or approval of the use of such commercial hardware or software.

UNCLASSIFIED
Security Classification

DOCUMENT CONTROL DATA - R & D

(Security classification of title, body of abstract and indexing annotation must be entered when the overall report is classified)

1. ORIGINATING ACTIVITY *(Corporate author)* Aeroballistics Directorate Directorate for Research, Development, Engineering and Missile Systems Laboratory U. S. Army Missile Command Redstone Arsenal, Alabama 35809	2a. REPORT SECURITY CLASSIFICATION Unclassified 2b. GROUP N/A

3. REPORT TITLE

ROCKET PLUME EFFECTS ON BOATTAIL AND FLARE BODIES OF REVOLUTION AT TRANSONIC SPEEDS

4. DESCRIPTIVE NOTES *(Type of report and inclusive dates)*

Technical Report

5. AUTHOR(S) *(First name, middle initial, last name)*

Donald V. Rubin

6. REPORT DATE 31 May 1971	7a. TOTAL NO. OF PAGES 48	7b. NO. OF REFS 2
8a. CONTRACT OR GRANT NO. b. PROJECT NO. (DA) 1M262303A214 c. AMC Management Structure Code No. 522C.11.214.05 d.	9a. ORIGINATOR'S REPORT NUMBER(S) RD-TR-71-17 9b. OTHER REPORT NO(S) *(Any other numbers that may be assigned this report)* AD	

10. DISTRIBUTION STATEMENT

Approved for public release; distribution unlimited.

11. SUPPLEMENTARY NOTES None	12. SPONSORING MILITARY ACTIVITY Same as No. 1

13. ABSTRACT

This report presents an analysis of the pressure data from a wind tunnel test conducted to gain information about rocket plume effects on missile base pressure and local pressure along flared and boattailed bodies of revolution at transonic speeds. ~~The test~~ was conducted ~~at $M_\infty = 0.5$ to 1.2~~. The jet plume was simulated by a cold air jet over a pressure range from 0 to approximately 600 psia.

DD FORM 1 NOV 65 1473 REPLACES DD FORM 1473, 1 JAN 64, WHICH IS OBSOLETE FOR ARMY USE.

UNCLASSIFIED
Security Classification

31 May 1971

Report No. TD-TR-71-17

ROCKET PLUME EFFECTS ON BOATTAIL AND FLARE BODIES OF REVOLUTION AT TRANSONIC SPEEDS

by

Donald V. Rubin

DA Project No. 1M262303A214
AMC Management Structure Code No. 525C.11.214.05

Approved for public release; distribution unlimited.

Aeroballistics Directorate
Directorate for Research, Development, Engineering
and Missile Systems Laboratory
U.S. Army Missile Command
Redstone Arsenal, Alabama 35809

ABSTRACT

This report presents an analysis of the pressure data from a wind tunnel test conducted to gain information about rocket plume effects on missile base pressure and local pressure along flared and boattailed bodies of revolution at transonic speeds. The test was conducted at $M_\infty = 0.5$ to 1.2. The jet plume was simulated by a cold air jet over a pressure range from 0 to approximately 600 psia.

CONTENTS

		Page
1.	Introduction	1
2.	Apparatus and Procedure	1
3.	Discussion	2
4.	Conclusions	6

ILLUSTRATIONS

Figure		Page
1	Model General Arrangement	7
2	Afterbody Configurations	8
3	Nozzle Configurations	9
4	Boattail Body Pressure Distribution Configuration B_3N_{12}, $M_\infty = 1.2$, $\alpha = 0$ Degree	10
5	Boattail Body Pressure Distribution Configuration B_3N_{12}, $M_\infty = 1.1$, $\alpha = 0$ Degree	11
6	Schlieren Photographs Configuration B_3N_{12}, $M_\infty = 1.2$, $\alpha = 0$ Degree	12
7	Boattail Body Pressure Distribution Configuration B_3N_{12}, $M_\infty = 1.0$, $\alpha = 0$ Degree	13
8	Boattail Body Pressure Distribution Configuration B_3N_{12}, $M_\infty = 0.9$, $\alpha = 0$ Degree	14
9	Boattail Body Pressure Distribution Configuration B_3N_{12}, $M_\infty = 0.7$, $\alpha = 0$ Degree	15
10	Schlieren Photographs Configuration B_3N_{12}, $M_\infty = 1.0$, $\alpha = 0$ Degree	16
11	Schlieren Photographs Configuration B_3N_{12}, $M_\infty = 0.9$, $\alpha = 0$ Degree	17
12	Local Mach Number Distribution Configuration B_3N_{12}, $M_\infty = 0.9$, $\alpha = 0$ Degree	18
13	Boattail Body Pressure Distribution at Angle of Attack Configuration B_3N_{12}, $M_\infty = 1.2$	19
14	Boattail Body Pressure Distribution at Angle of Attack Configuration B_3N_{12}, $M_\infty = 1.0$	20
15	Boattail Body Pressure Distribution at Angle of Attack Configuration B_3N_{12}, $M_\infty = 0.9$	21
16	Boattail $P/P_{\text{Power Off}}$ at Station $X/D = 0.025$ for Varying C_T	22
17	Boattail P_b/P_∞ Versus C_T	23

Figure		Page
18	Flare Body Pressure Distribution Configuration B_8N_1, $M_\infty = 1.2$, $\alpha = 0$ Degree	24
19	Flare Body Pressure Distribution Configuration B_8N_1, $M_\infty = 1.0$, $\alpha = 0$ Degree	25
20	Flare Body Pressure Distribution Configuration B_8N_1, $M_\infty = 0.9$, $\alpha = 0$ Degree	26
21	Flare Body Pressure Distribution Configuration B_8N_{14}, $M_\infty = 1.2$, $\alpha = 0$ Degree	27
22	Flare Body Pressure Distribution Configuration B_8N_{14}, $M_\infty = 1.0$, $\alpha = 0$ Degree	28
23	Flare Body Pressure Distribution Configuration B_8N_{14}, $M_\infty = 0.9$, $\alpha = 0$ Degree	29
24	Schlieren Photographs Configuration B_8N_{14}, $M_\infty = 1.2$, $\alpha = 0$ Degree	30
25	Flare Body Pressure Distribution at Angle of Attack Configuration B_8N_{14}, $M_\infty = 1.2$	31
26	Flare Body Pressure Distribution at Angle of Attack Configuration B_8N_{14}, $M_\infty = 1.0$	32
27	Flare Body Pressure Distribution at Angle of Attack Configuration B_8N_{14}, $M_\infty = 0.9$	33
28	Flare $P/P_{Power\ Off}$ at Station $X/D = 0.025$ for Varying C_T	34
29	Flare P_b/P_∞ Versus C_T	35
30	Proportionality Factor as a Function of Base Area Ratio	36

SYMBOLS

A_j	Area of jet at exit plane	(in.^{2})
A_b	Body base area	(in.^{2})
A_c	Body cylinder cross sectional area	(in.^{2})
C_T	Nozzle thrust force coefficient, $\frac{\text{thrust}}{q_\infty A_B} = \frac{\gamma_j P_j A_j M_j^2 + A_j(P_j - P_\infty)}{0.5\ \gamma_\infty P_\infty A_B M_\infty^2}$	
D^*	Nozzle throat diameter	(in.)
D	Reference diameter = 2.50 in.	(in.)
D_b	Base diameter	(in.)
D_j	Nozzle exit diameter	(in.)
$\dot{m}$	Weight flow through nozzle	(lb/sec)
M_j	Nozzle design Mach number	
M_{Local}	Local Mach number	
M_∞	Freestream Mach number	
P_c	Nozzle chamber pressure	(psia)
P_∞	Freestream static pressure	(psia)
P_b/P_∞	Measured base pressure over freestream static pressure	
P_c/P_∞	Nozzle chamber pressure over freestream static pressure	
$P/P_{Power\ Off}$	Measured orifice pressure over-orifice pressure for power-off	
P_{b_c}/P_b	Measured cylinder base pressure over flare or boattail base pressure	
$\frac{R_b - r}{D_b}$	$\frac{\text{Base radius - orifice radius from model ℄}}{\text{Base Diameter}}$	

X/D	Distance forward of base along ℄ over reference diameter	
α, ALPHA	Model angle of attack (positive nose up)	(deg)
θ_b	Boattail or flare angle	(deg)
θ_j	Nozzle angle at exit plane	(deg)
γ_j	Ratio specific heat jet	
γ_∞	Ratio specific heat freestream	
q_∞	Freestream dynamic pressure	(psia)

1. Introduction

Flow separation over the aft end of missiles caused by rocket plumes has resulted in aerodynamic problems associated with a loss in stability and control effectiveness. To investigate these aerodynamic problems, a transonic wind tunnel test was conducted at freestream Mach numbers of 0.5 to 1.2 using boattailed and flared afterbody missiles at high jet thrust levels. The jet exhaust plume was generated by a cold air jet using a pressure range from 0 to approximately 600 psia with three different thrust nozzles. The purpose of this investigation was to gain more general information about rocket plume effects on the missile base pressure and local pressure along flared and boattailed afterbodies, and to determine the dependency of base pressure on base diameter in the transonic region as a function of jet thrust levels. This report presents an analysis of the pressure data from this wind tunnel test.

The basic data from the test was reported by Rubin[1].

2. Apparatus and Procedure

The tests were conducted in the Cornell Aeronautical Laboratories (CAL) 8-foot transonic wind tunnel. The tunnel Mach number range was varied from 0.5 to 1.2. All tests were run in a "constant-mass" mode with a wind-off total pressure of 1/2 atmosphere. The "constant-mass" implies that the total air mass in the tunnel circuit remains constant, and that no mass removal or addition is required for changes in test section Mach number.

The model is a body of revolution, 2.5 inches in diameter, with a 4-caliber tangent ogive nose, a 5.5-caliber cylindrical centerbody, and eight interchangeable 3.5-caliber afterbody configurations. Cold dry air flowing through a nozzle in the body base simulated the rocket exhaust flow. The cold air was supplied to the nozzle through a hollow swept strut, which housed the instrumentation lines and supported the model from the standard sting support system of the CAL facility. The model instrumentation consisted of static and total pressure orifices. A sketch of the general arrangement of the model and strut is shown in Figure 1.

Eight afterbody configurations were tested, four were boattails, three were flares, and one was cylindrical. These afterbodies are shown in Figure 2.

---

[1]Rubin, Donald V., A Transonic Investigation of Jet Plume Effects on Base and Afterbody Pressures of Boattail and Flare Bodies of Revolution, U. S. Army Missile Command, Redstone Arsenal, Alabama, Report No. RD-TR-70-10, October 1970.

Three nozzles were used with the afterbody configurations; nozzle N_1 and N_{14} with the flared afterbodies and N_{12} with the boattailed afterbodies. Nozzle N_1 and N_{12} were designed for a jet exit Mach number of 2.7 and a conical expansion angle of 20 degrees. Nozzle N_{14} is a sonic nozzle having an exit Mach number of 1.0 The nozzle configurations are shown in Figure 3.

3. Discussion

a. General Data

The fluctuation in local body pressures upstream of the boattail and flare configurations indicate there may be an interference effect from the model strut support sting. This is indicated by the variation in pressure from freestream at stations upstream of the boattail in Figures 4 and 5. Also the strut support sting interference may be indicated in the schlieren photographs presented in Figure 6 along the lower part of the cylinder for $M_\infty = 1.2$. The overall trend and the incremental change in the data are not affected by any localized interference from the support sting.

The boundary layer was measured by a pitot static tube at points upstream of the flare and boattail junctions for configurations B3 and B9 at $M_\infty = 0.7$ to 1.2 for jet-off cases. In all cases the boundary layer was turbulent and matched a 1/7 power velocity profile.

b. Boattails

Body pressure distributions along boattail configuration B_3N_{12}, for changing jet pressure ratios are shown in Figures 4 through 9. Corresponding schlieren photographs for varying P_c/P_∞ and M_∞ are presented in Figures 6, 10, and 11.

The jet pressure ratio, P_c/P_∞, has a great influence on the boattail body pressure distribution. As P_c/P_∞ is increased, flow separation is induced along the boattail. For $M_\infty \geq 1.0$, Figures 4, 5, and 7 show that at or near the boattail expansion corner the body pressure for power-on cases decreases to the original power-off pressure distribution. The $M_\infty = 0.9$ (Figure 8) case also indicates the same type of pressure recovery.

The series of schlieren photographs in Figure 6 show the shock from the jet plume initially off the body at $M_\infty = 1.2$. As the jet pressure increases, the jet plume shock moves upstream attaching to the boattail. As the jet pressure increases, the shock moves further upstream towards the boattail expansion corner. A comparison of the local body pressures in Figure 4 indicates that the shock from the jet plume attaches to the boattail when the base pressure exceeds the pressure level upstream of the corner.

The schlieren photographs in Figure 10 for $M_\infty = 1.0$ correlate with the boattail body pressure distributions in Figure 7. Initially for the power-off condition, the shock from the boattail recompression is attached to the boattail. As the jet pressure increases, the recompression shock is drawn toward the base. For a $P_c/P_\infty = 23.7$, the boattail pressure distribution is lower than the pressure distribution for the power-off case. The schlieren photograph indicates that the boattail recompression shock is interacting with the base area. As the jet pressure is increased, the recompression shock is pushed back upstream along the boattail until the shock approaches the corner. When the shock approaches the corner, it interacts with the boattail expansion fan. For $P_c/P_\infty = 133.5$, the schlieren indicates the shock is at the corner and the boattail expansion fan has nearly been eliminated. The body pressure distribution shows the body pressure recovery occurs at the boattail expansion corner.

Figure 11 shows the corresponding schlieren photographs for the boattail pressure data in Figure 8 for $M_\infty = 0.9$. A plot (Figure 12) of local Mach number distribution for the $M_\infty = 0.9$ indicates that the flow just ahead of the corner is supersonic and that a shock develops on the boattail downstream of the corner. The schlieren photographs also indicate that a weak lambda shock is formed on the boattail for the power-off condition. The lambda shock is moved upstream as the jet pressure is increased, until $P_c/P_\infty > 79$ when the lambda shock is pushed past the expansion corner. This is indicated in the body pressure data for $P_c/P_\infty = 121$ where the pressure recovery occurs upstream of the corner.

Pressure distributions along boattail B_3N_{12} at ±2 degrees angle of attack are shown for $M_\infty = 1.2$, 1.0, and 0.9 in Figures 13, 14, and 15. For $M_\infty = 1.2$, there is negative lift on the cylinder for approximately 2 calibers upstream of the boattail junction. This is indicated where the positive angle-of-attack leeside pressure distribution is greater than the negative angle-of-attack windward pressure distribution indicated by cross hatched lines in Figure 13.

The influence on the boattail pressure at station X/D = 0.0025 caliber from the base because of the thrust coefficient, C_T, is shown in Figure 16. For the supersonic cases, the pressure ratio slope change could indicate a flow separation. Boattails B_3 and B_6 show this trend. For the subsonic $M_\infty = 0.9$, this pressure sepration trend is again indicated at a C_T level of 10 for the B_3 and B_6 afterbodies. The local pressure ratio is influenced by the boattail geometry and magnitude of the thrust coefficient.

A comparison of the boattail base pressure ratio with varying thrust coefficient is shown in Figure 17. An indication of where flow separation occurs is where the base pressure ratio, P_b/P_∞, changes slope. This point occurs at different thrust levles for each configuration. The separation points occur at approximately $C_T > 4$ for $M_\infty = 1.2$, $C_T > 6$ for $M_\infty = 1.0$, $C_T > 14$ for $M_\infty = 0.9$, and $C_T > 20$ for $M_\infty = 0.7$. A trend is established; however, there is not enough data to generalize the effects of thrust and M_∞ on boattail flow separation.

In general the effect of the boattail diameter ratio on the thrust coefficient is very apparent through the transonic range. As the base diameter ratio increases, the base pressure coefficient decreases for a given thrust level. Within the region of no upstream separation, the boattail base pressure is proportional to the boattail base diameter ratio.

c. Flares

The influence of the jet pressure ratio on a flared afterbody pressure distribution is shown in Figures 18 through 23. Comparisons are made for Configuration B_8 with two different jet nozzles. The $M_\infty = 1.2$ case shows a definite influence on the body pressure distribution because of the jet pressure ratio. Figures 18 and 21 indicate that nozzle M_j has a very large influence on local body pressure. As M_∞ decreases, the jet pressure ratio for both nozzles affect the local body pressure further upstream.

The schlieren photographs in Figure 24 show the effect of varying jet pressure ratio on Configuration B_8N_{14} for $M_\infty = 1.2$. The shock from the jet plume is shown moving upstream along the body and finally coalescing with the shock from the flare compression corner. It can be noted that the shape of the compression shock changes after the jet plume shock has converged. The local body pressure distribution for

this case is shown in Figure 21. Correlation of the pressure data with the schlieren photographs indicates that separation has been induced along the flare. For $P_c/P_\infty = 54.6$, the schlieren shows the shock from the jet plume attached to the flare, and the local body pressure indicates the start of separation.

Local pressure distributions for flare Configuration B_8N_{14} at ±2 degrees angle of attack is shown in Figures 25, 26, and 27. Over the M_∞ range, for the power-off and power-on cases, the windward pressure distribution is greater than the leeward pressure distribution indicating that positive lift is generated along the flare. For the $M_\infty = 1.2$ case (Figure 25), there is negative lift generated just upstream of the flare corner. This negative lift region may be a zone of separated flow.

The effect of the jet pressure ratio on the local pressure at station X/D = 0.025 caliber from the flare base is shown in Figure 28. The dominant effects on the local body pressure are shown: nozzle M_j, flare base diameter, and freestream Mach number. At each M_∞ flare, pressure separation is a function of the base geometry and nozzle M_j. The configuration with the most localized effect from the jet plume was the minimum diameter flare with the sonic nozzle, Configuration B_9N_{14}. Flow separation points are indicated by slope changes. For example, flow separation is indicated for Configuration B_9N_{14} at a $C_T = 32$ for $M_\infty = 1.2$.

The effect of the thrust coefficient on base pressure for the flare configurations is shown in Figure 29. A change in the slope of the base pressure curves indicate separation. This separation is a function of base diameter and nozzle M_j.

d. Proportionality Factor

A correlation parameter, reported by Rubin[2], et al. using the base area and base pressure of a cylindrical afterbody is presented in Figure 30. All data presented are for nonseparated conditions. The boattail configurations correlate with the cylindrical base

---

[1]Rubin, D. V., Brazzel, C. E., and Henderson, J. H.; The Effects of Jet Plume and Boattail Geometry on Base and Afterbody Pressures of a Body of Revolution at Mach Number 2.0 to 3.5; U. S. Army Missile Command, Redstone Arsenal, Alabama, Report No. RD-TR-70-5, April 1970.

area and base pressure through the transonic region. However, at subsonic speeds the correlation breaks down. The flare base pressure does not correlate using the cylindrical base pressure and base area as a proportionality factor in the transonic region. At $M_\infty = 1.2$ the proportionality factor starts to become an influencing parameter in correlating flare base pressure.

The correlation method does not predict base pressures for boattail or flare afterbodies when flow separation occurs.

4. Conclusions

The following conclusions were made from an analysis of the test results.

a. Boattail

1) Boattail base pressure in the transonic region can be correlated by using the base area and base pressure of a cylindrical afterbody for values of thrust coefficients where flow separation does not occur. At subsonic speeds, base pressures cannot be correlated by this method.

2) At Mach number ≥ 0.9, the boattail body pressure distribution for power-on cases decreases to the original power-off pressure distribution at the boattail expansion corner.

3) For the $M_\infty = 0.9$ case, local supersonic flow is established upstream of the expansion corner causing supersonic flow along the boattail and the generation of a lambda shockwave.

4) Flow separation is a function of thrust coefficient and M_∞. A change in slope of the base pressure versus C_T curve indicates that flow separation occurs. More data should be obtained to generalize the effects of C_T and M_∞ on boattail flow separation.

b. Flares

1) In the transonic range, flare base pressure cannot be correlated using cylindrical base pressure and base area.

2) At $M_\infty = 1.2$, the flare base pressure starts to be in the range where the base area ratio can be used as a correlation parameter for the nonseparated cases.

3) At a given M_∞, flare flow separation is a function of base geometry and thrust coefficient, C_T.

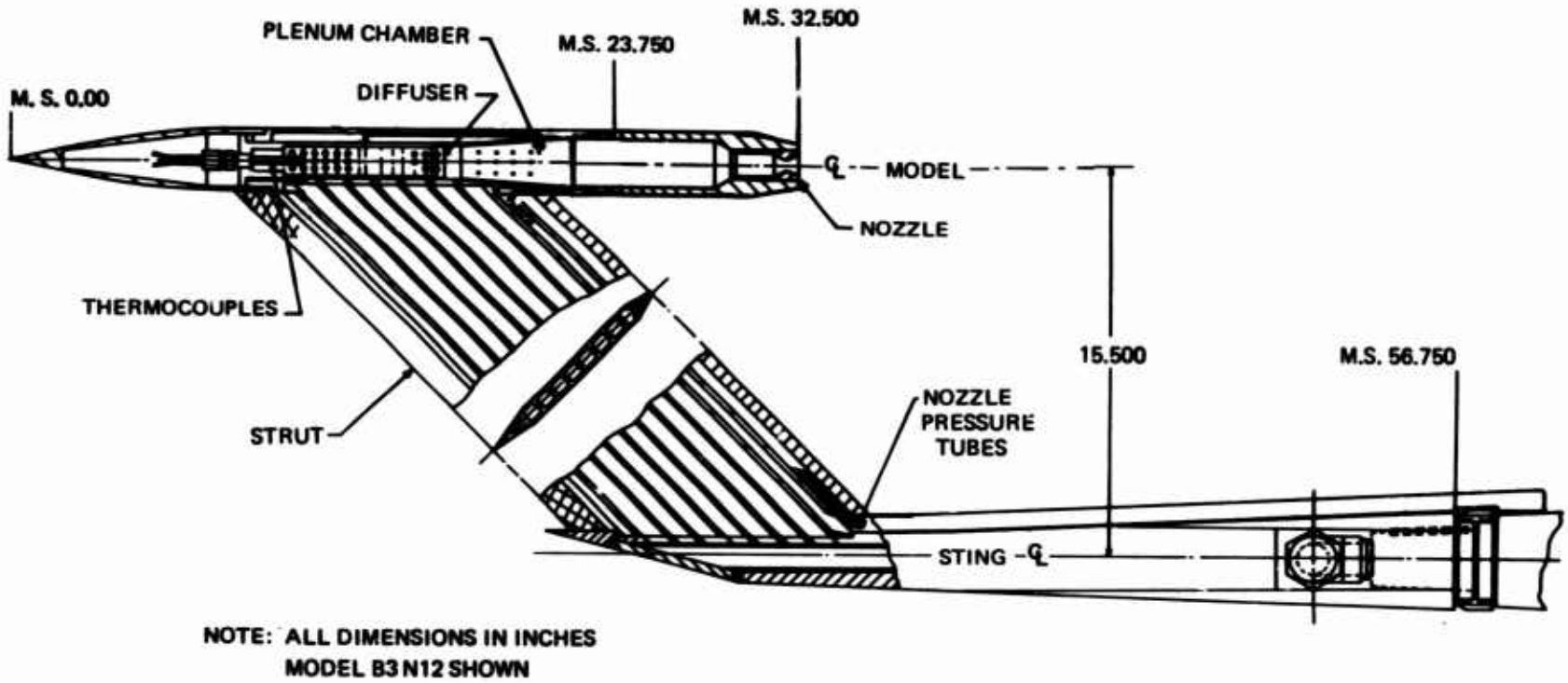

Figure 1. Model General Arrangement

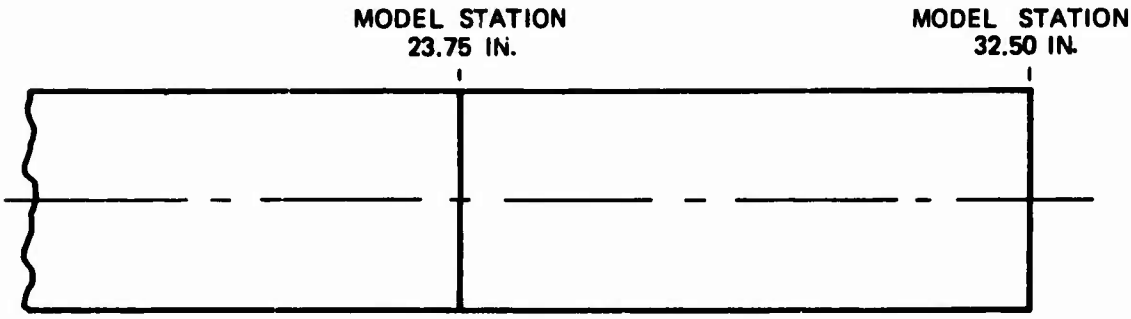

A. BODY CONFIGURATION B_1

BODY	L_b (IN.)	D_b (IN.)	L_b/D	D_b/D	θ_b (DEG.)
B_3	2.045	1.818	0.818	0.727	9.467
B_4	2.045	2.045	0.818	0.818	6.348
B_5	2.045	2.273	0.818	0.909	3.177
B_6	3.066	1.818	1.226	0.727	6.346

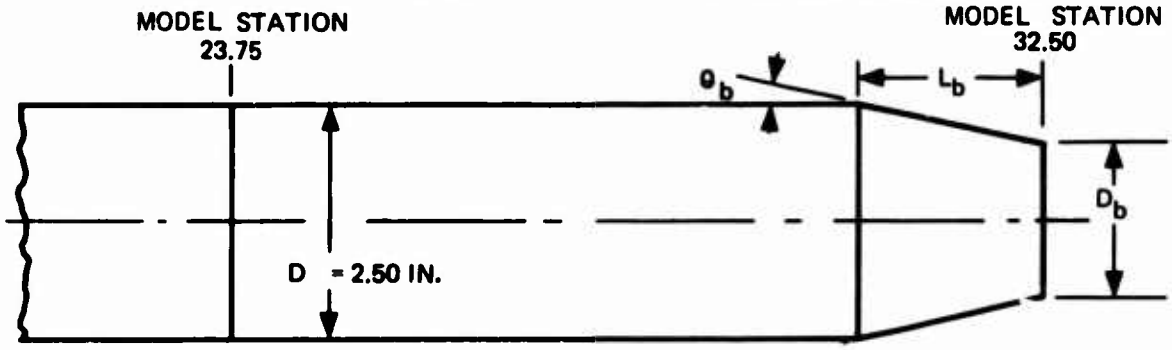

B. BOATTAILED AFTERBODIES

BODY	L_b (IN.)	D_b (IN.)	L_b/D	D_b/D	θ_b (DEG.)
B_7	7.50	3.360	3.000	1.344	3.281
B_8	3.75	3.360	1.500	1.344	6.541
B_9	3.75	2.930	1.500	1.172	3.281

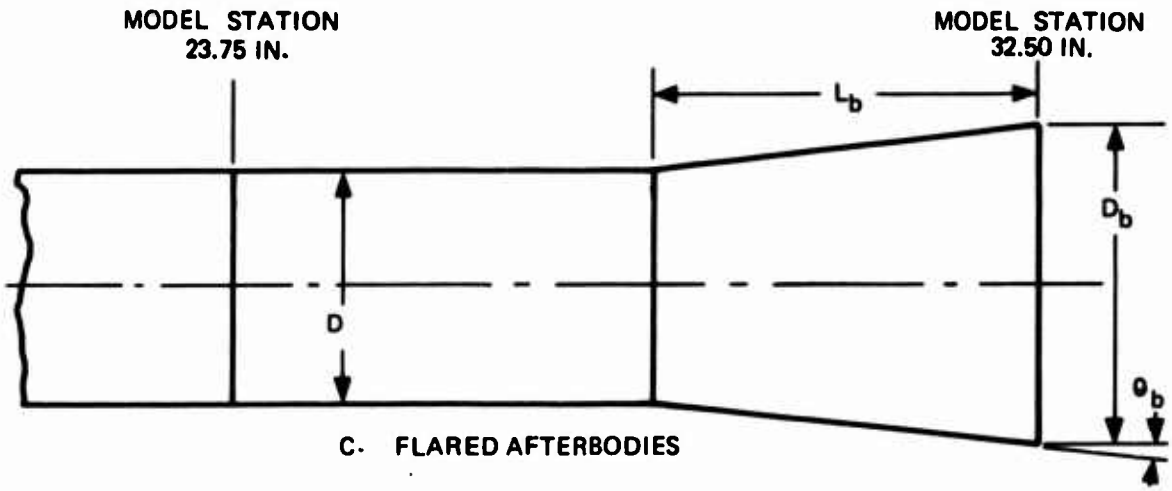

C. FLARED AFTERBODIES

Figure 2. Afterbody Configurations

NOZZLE	D_j (IN.)	D_j / D
14 (1.0 - 0 - 0.60)	1.500	0.600

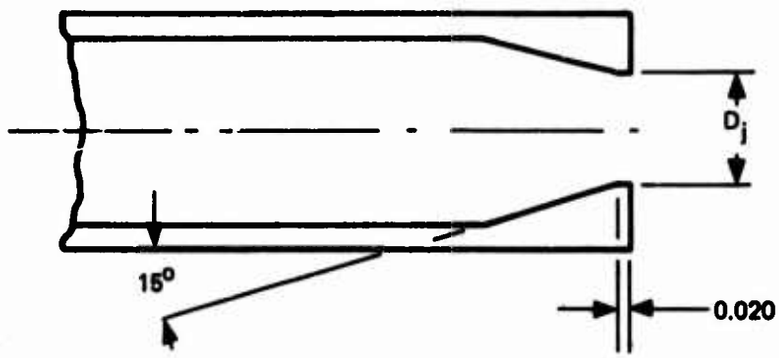

A. SONIC NOZZLES

NOZZLE	D* (IN.)	D_j (IN.)	L (IN.)	R (IN.)	θ_j(DEG)	D_j / D
1 (2.7 - 20 - 0.80)	1.123	2.004	1.309	0.562	20	0.800
12 (2.7 - 20 - 0.45)	0.6305	1.125	0.735	0.315	20	0.450

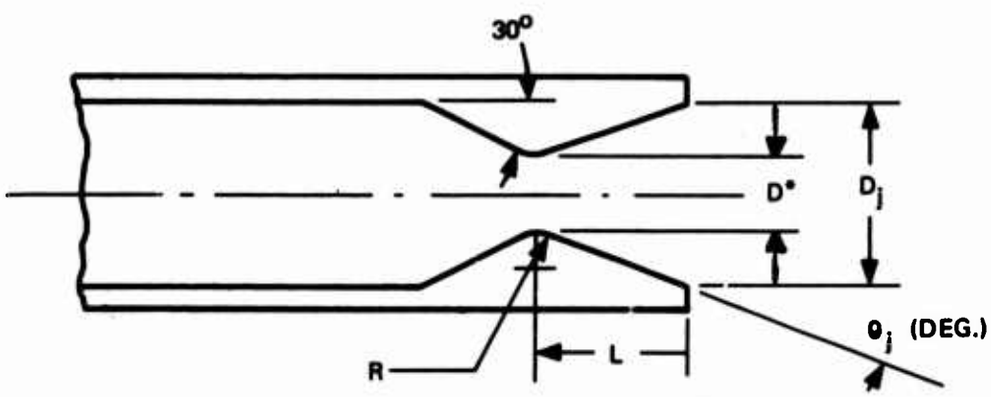

B. CONICAL NOZZLES

Figure 3. Nozzle Configurations

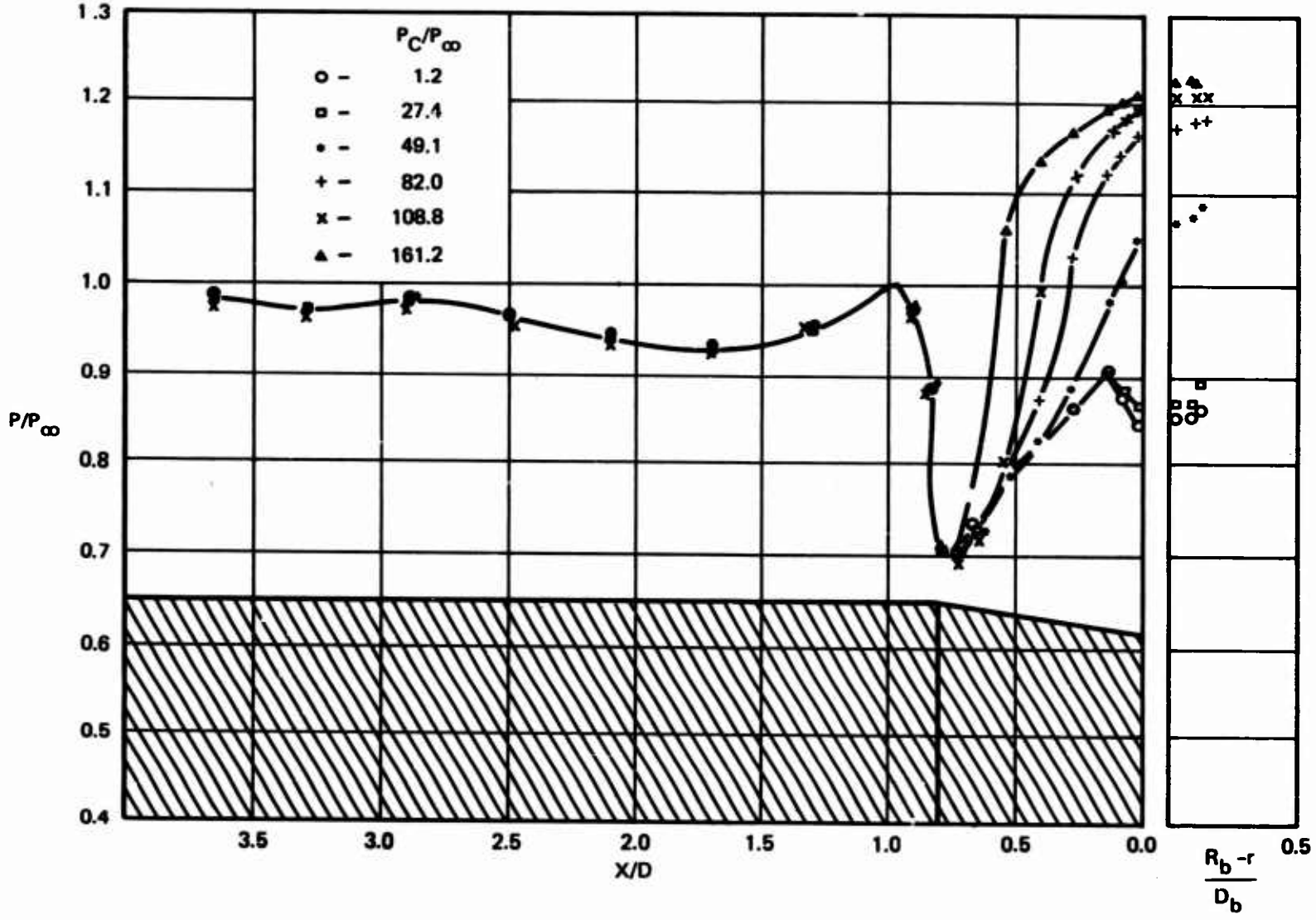

Figure 4. Boattail Body Pressure Distribution Configuration B_3 N_{12}, $M_\infty = 1.2$, $\alpha = 0$ Degree

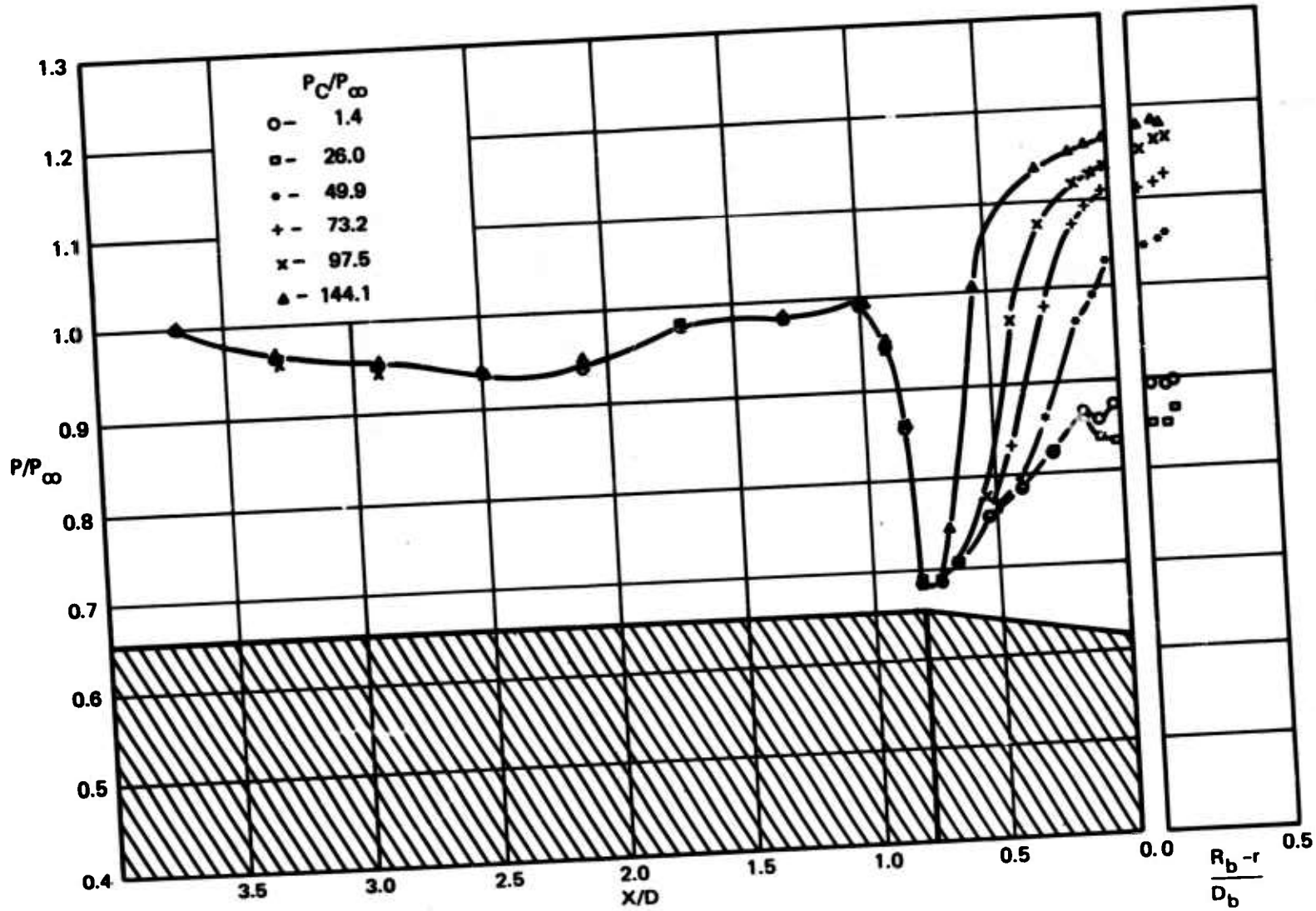

Figure 5. Boattail Body Pressure Distribution Configuration B_3N_{12}, $M_\infty = 1.1$, $\alpha = 0$ Degree

$P_C/P_\infty = 1.2$

$P_C/P_\infty = 27.4$

$P_C/P_\infty = 49.1$

$P_C/P_\infty = 82.0$

$P_C/P_\infty = 108.8$

$P_C/P_\infty = 136.6$

Figure 6. Schlieren Photographs Configuration B_3N_{12}, $M_\infty = 1.2$, $\alpha = 0$ Degree

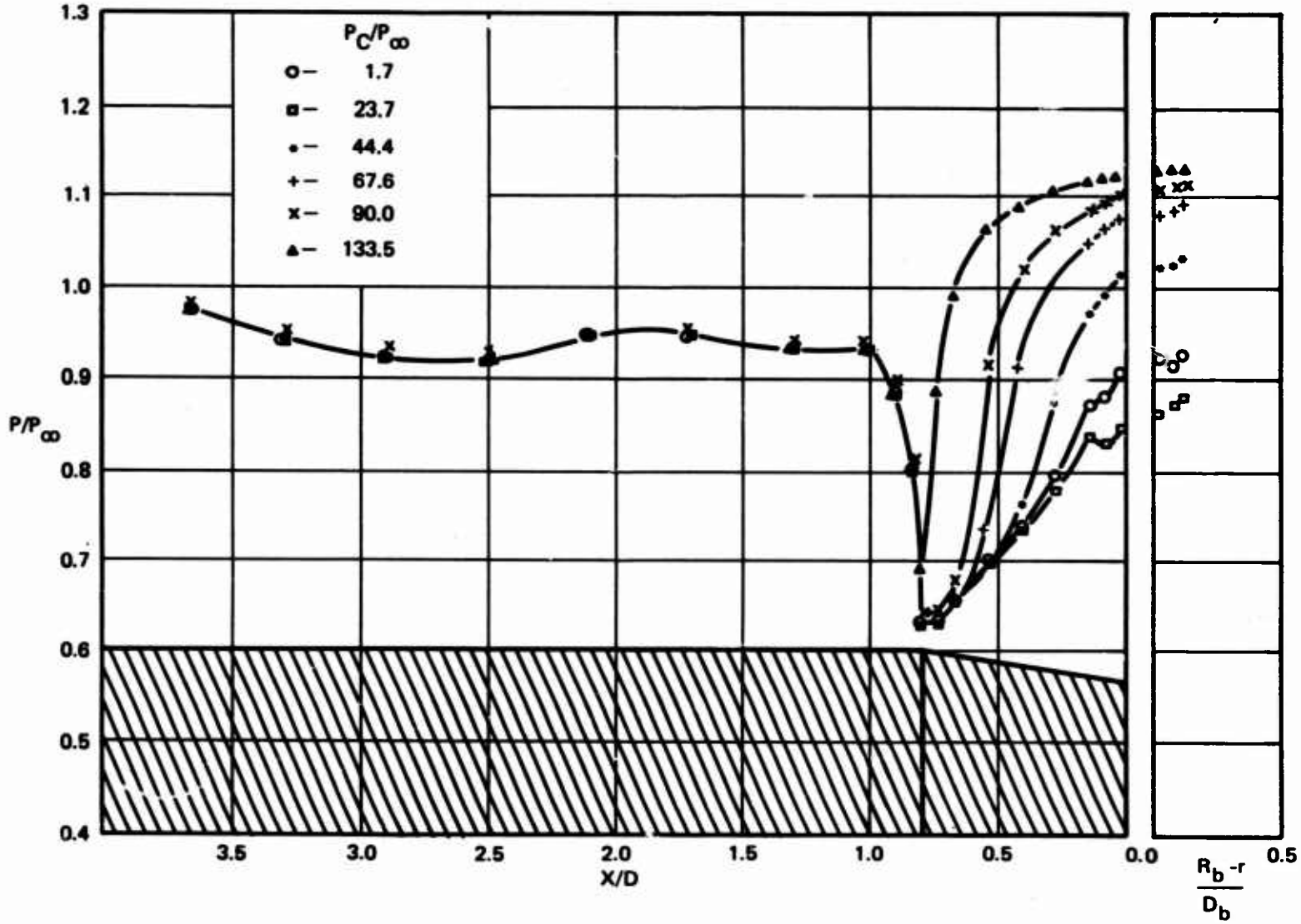

Figure 7. Boattail Body Pressure Distribution Configuration B_3N_{12}, $M_\infty = 1.0$, $\alpha = 0$ Degree

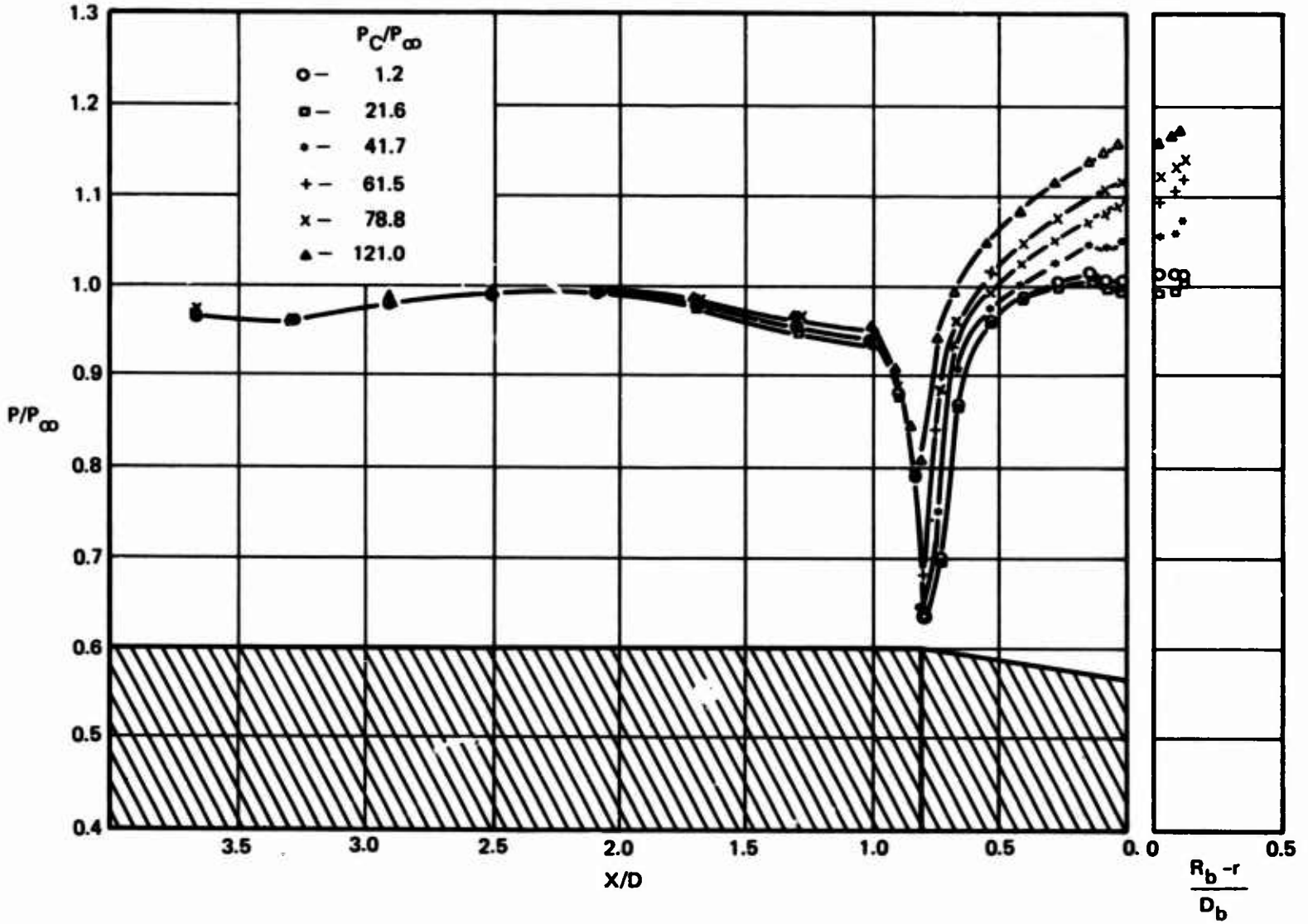

Figure 8. Boattail Body Pressure Distribution Configuration B_3N_{12}, $M_\infty = 0.9$, $\alpha = 0$ Degree

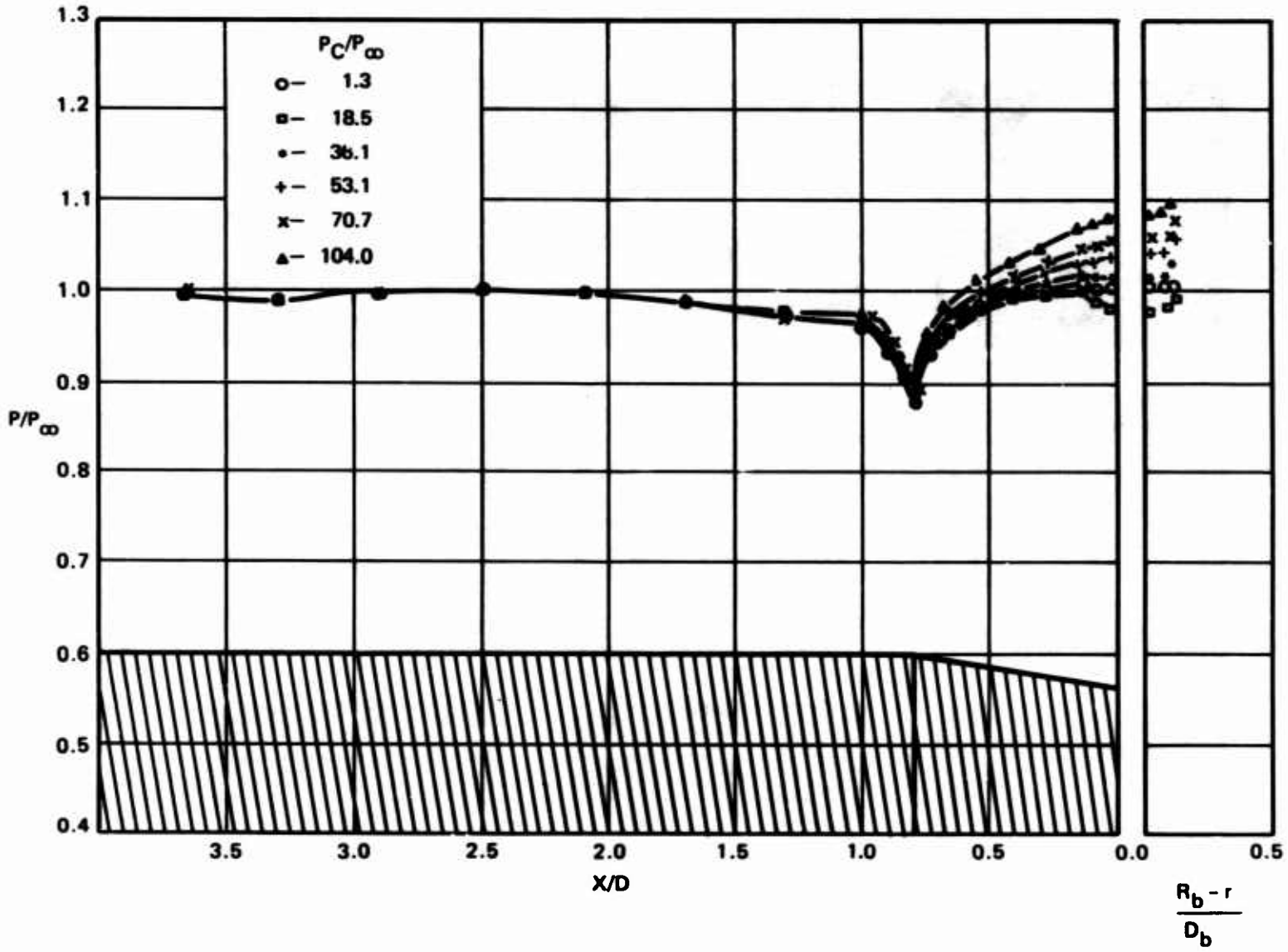

Figure 9. Boattail Body Pressure Distribution Configuration B_3N_{12}, $M_\infty = 0.7$, $\alpha = 0$ Degree

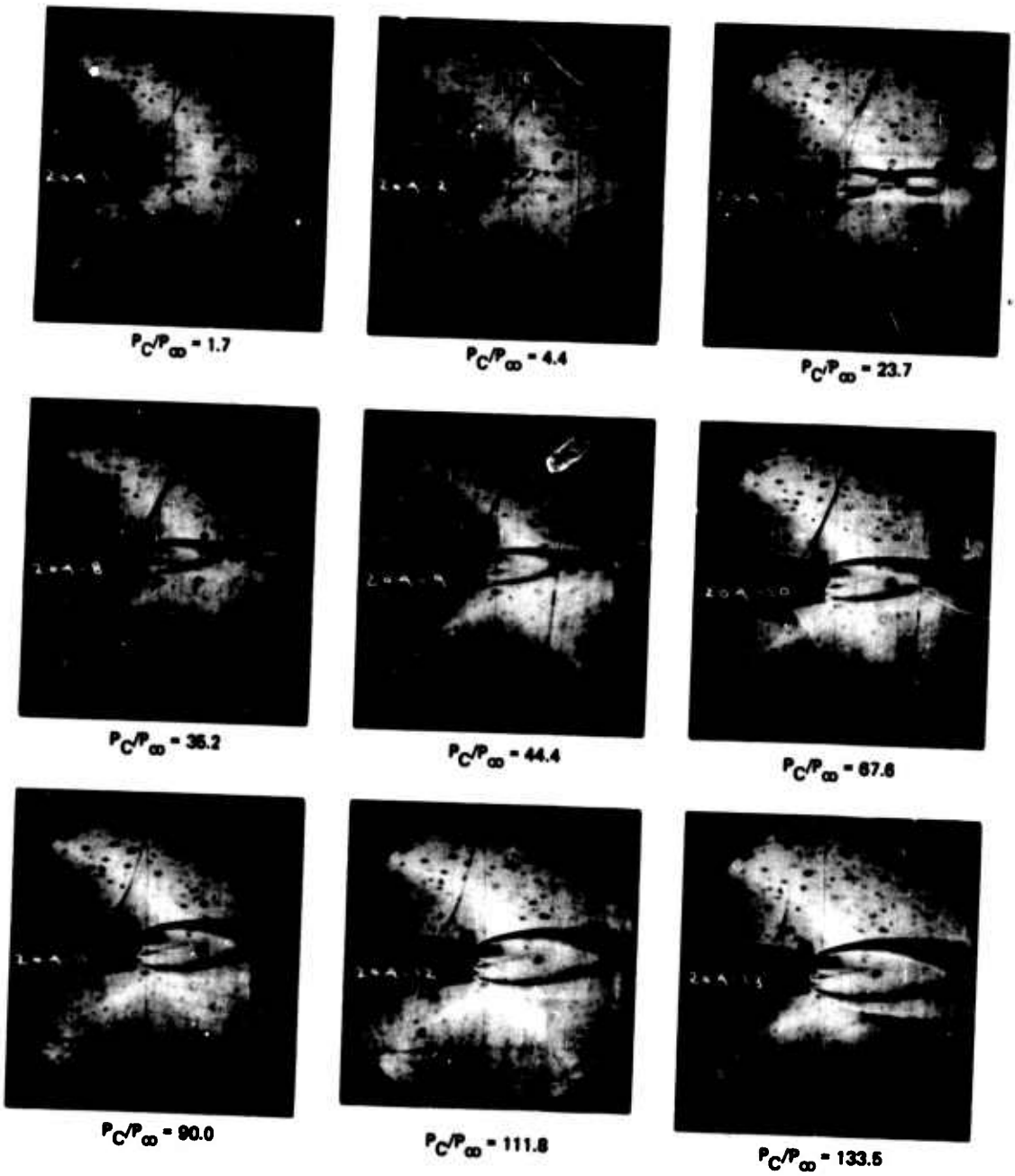

Figure 10. Schlieren Photographs Configuration B_3N_{12}, M_∞ = 1.0, α = 0 Degree

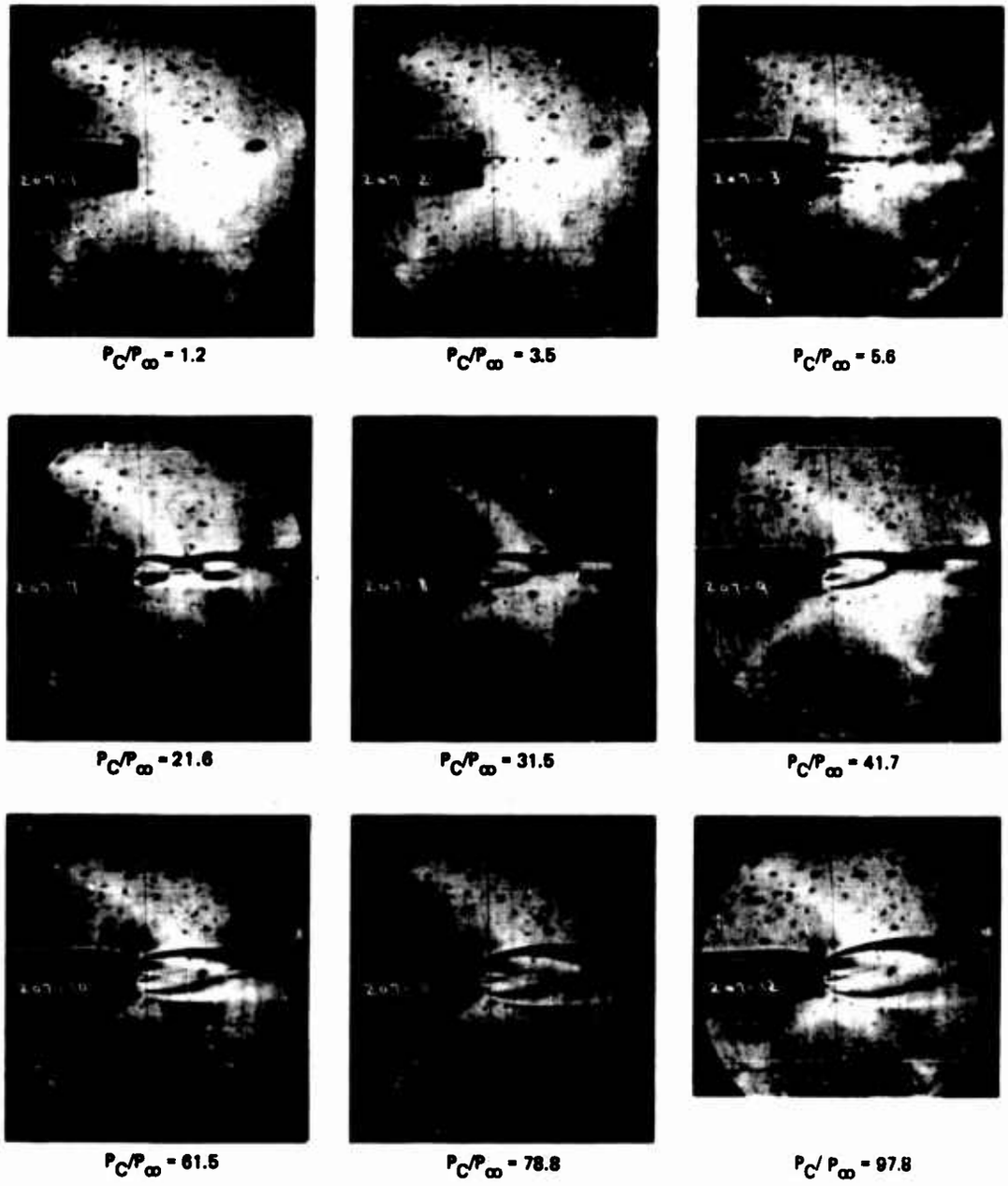

Figure 11. Schlieren Photographs Configuration B_3N_{12}, M_∞ = 0.9, α = 0 Degree

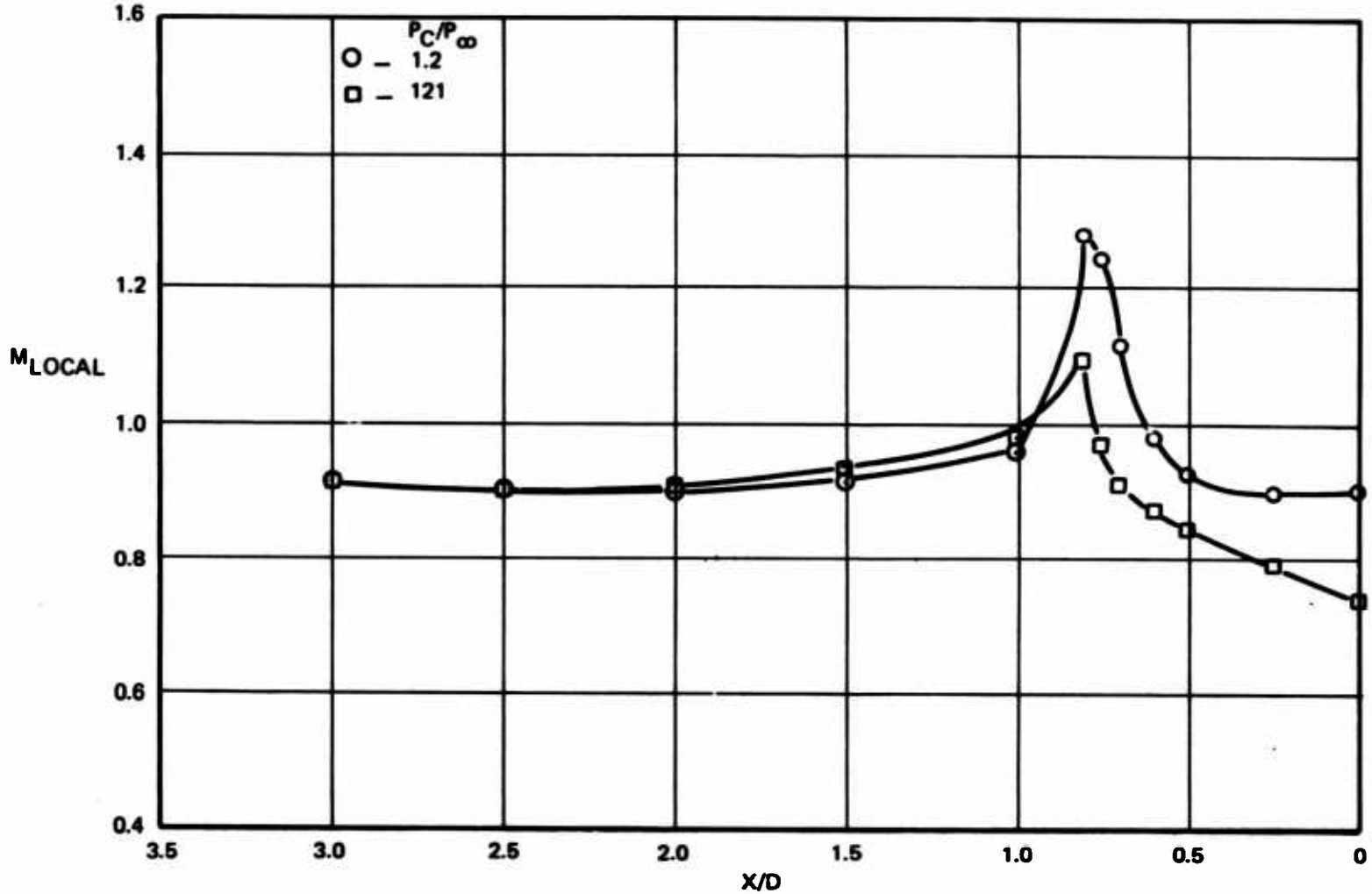

Figure 12. Local Mach Number Distribution Configuration B_3N_{12}, $M_\infty = 0.9$, $\alpha = 0$ Degree

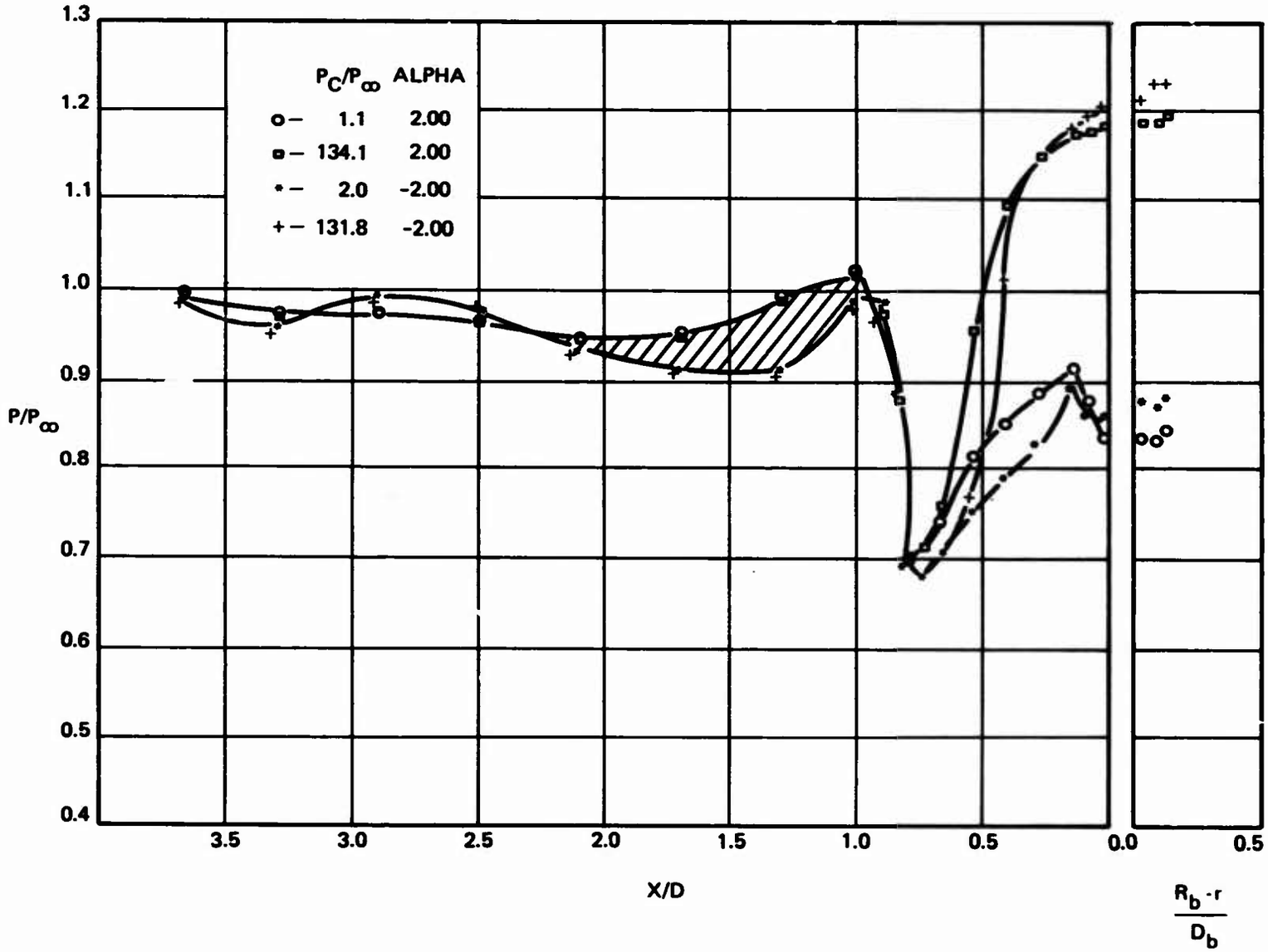

Figure 13. Boattail Body Pressure Distribution at Angle of Attack Configuration B_3N_{12}, $M_\infty = 1.2$

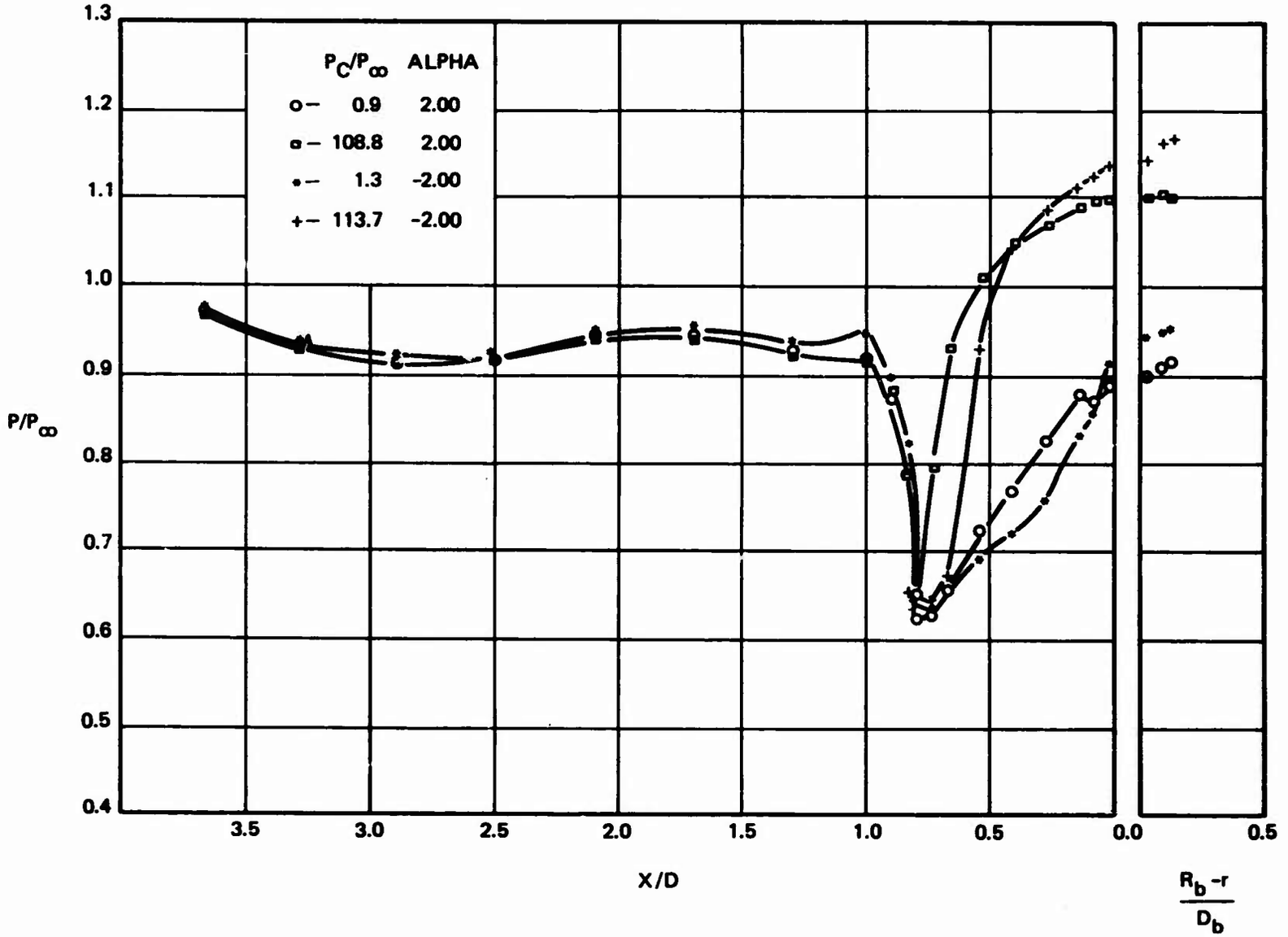

Figure 14. Boattail Body Pressure Distribution at Angle of Attack Configuration B_3N_{12}, $M_\infty = 1.0$

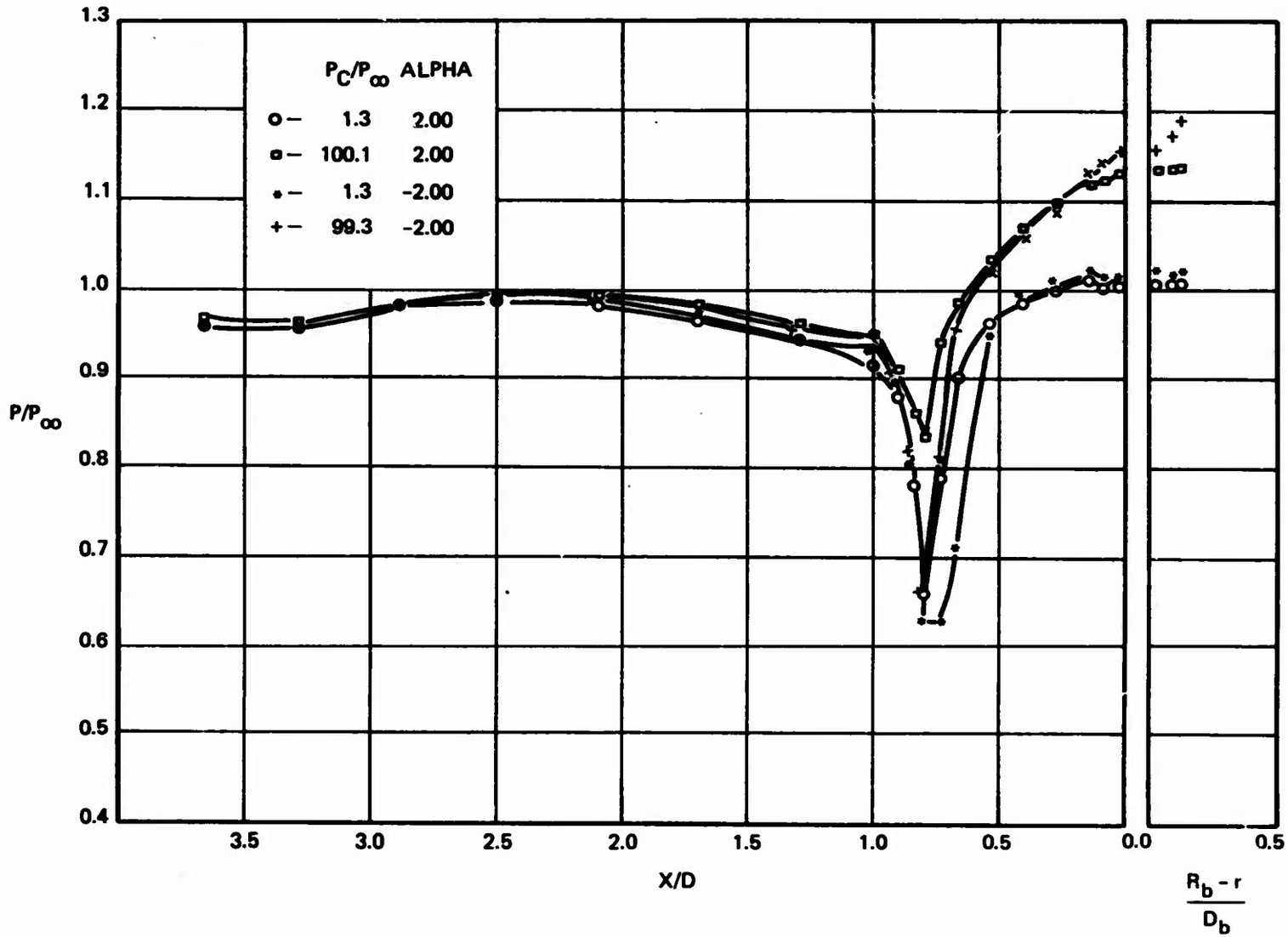

Figure 15. Boattail Body Pressure Distribution at Angle of Attack Configuration B_3N_{12}, $M_\infty = 0.9$

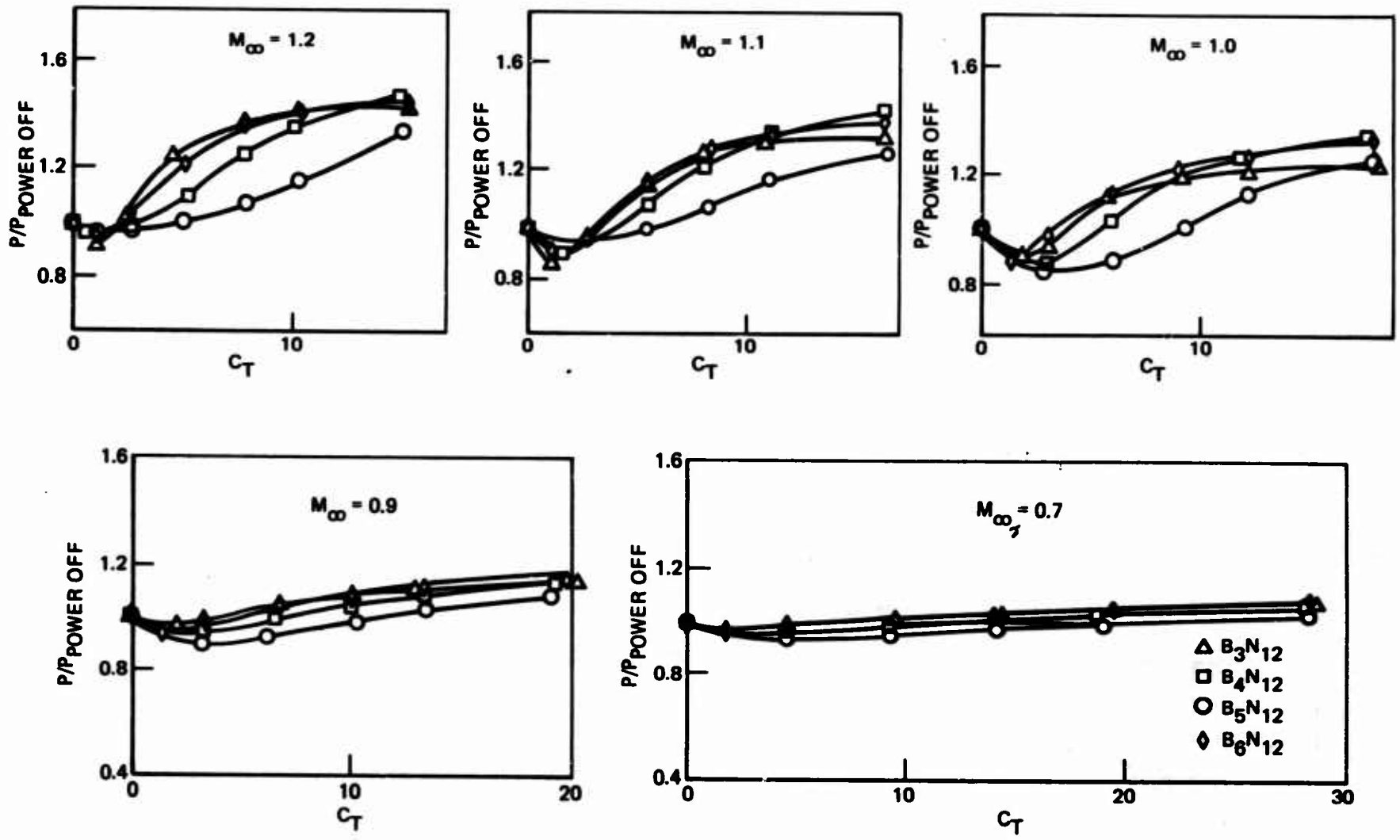

Figure 16. Boattail $P/P_{Power\ Off}$ at Station X/D = 0.025 for Varying C_T

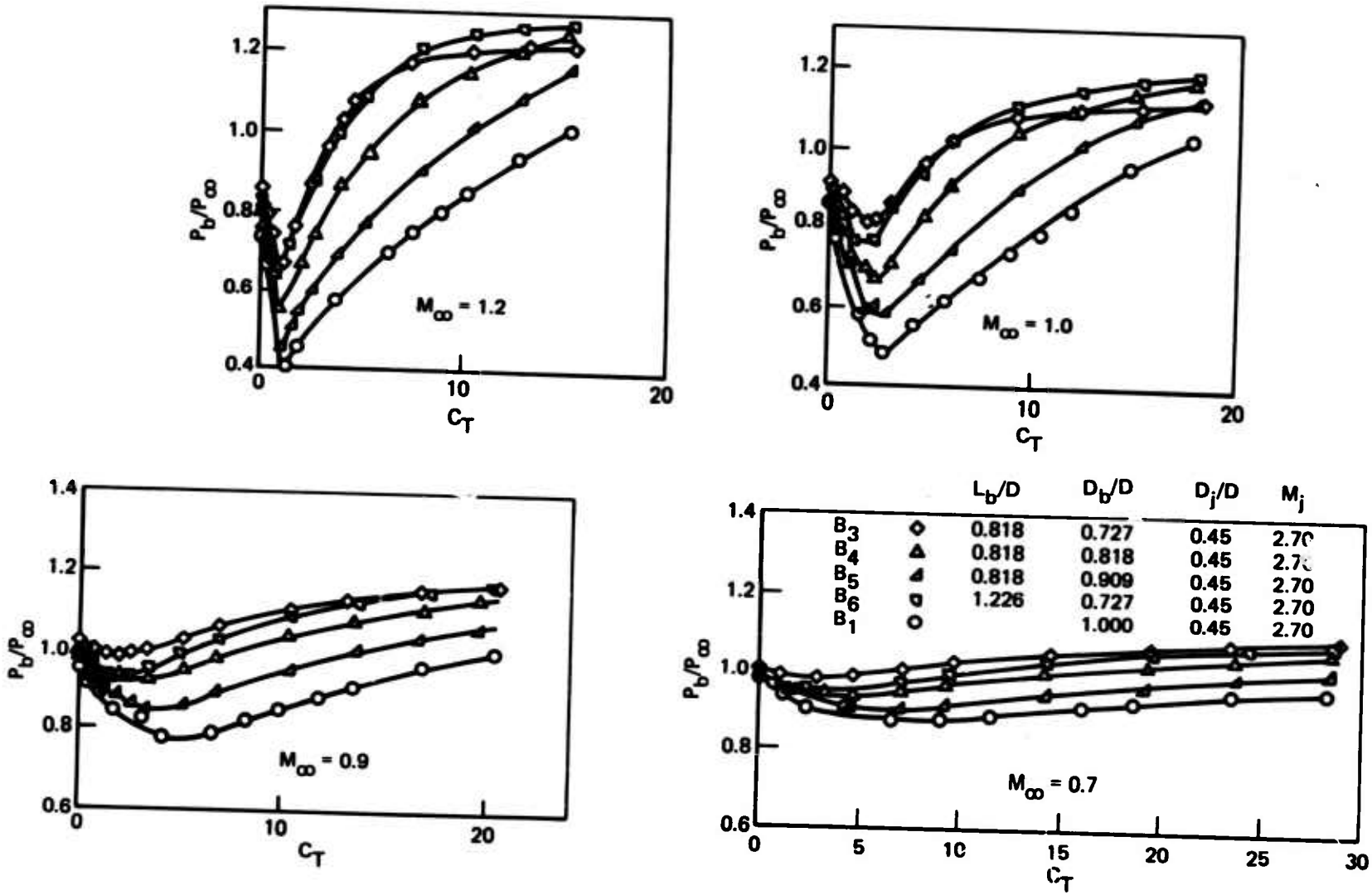

Figure 17. Boattail P_b/P_∞ Versus C_T

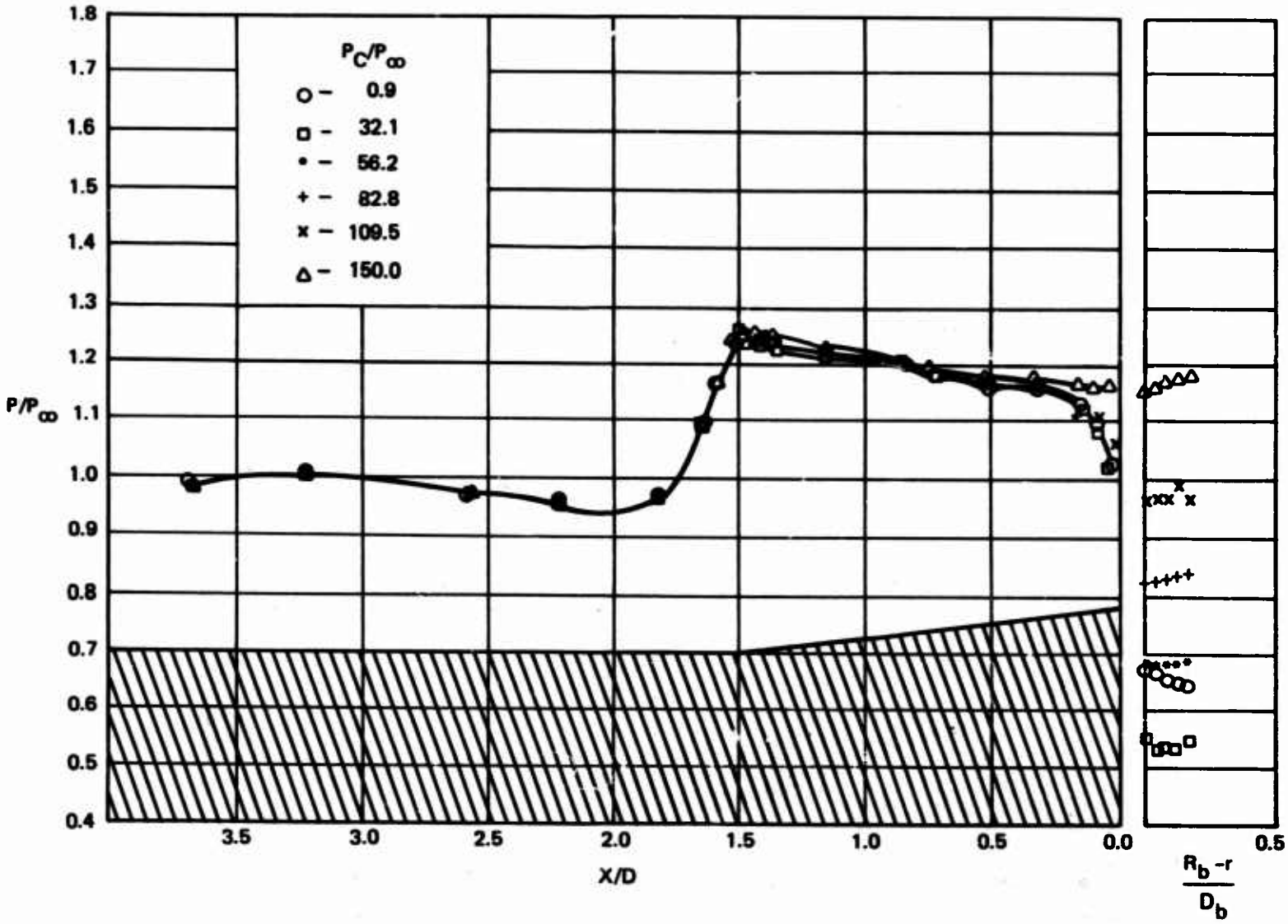

Figure 18. Flare Body Pressure Distribution Configuration B_8N_1, $M_\infty = 1.2$, $\alpha = 0$ Degree

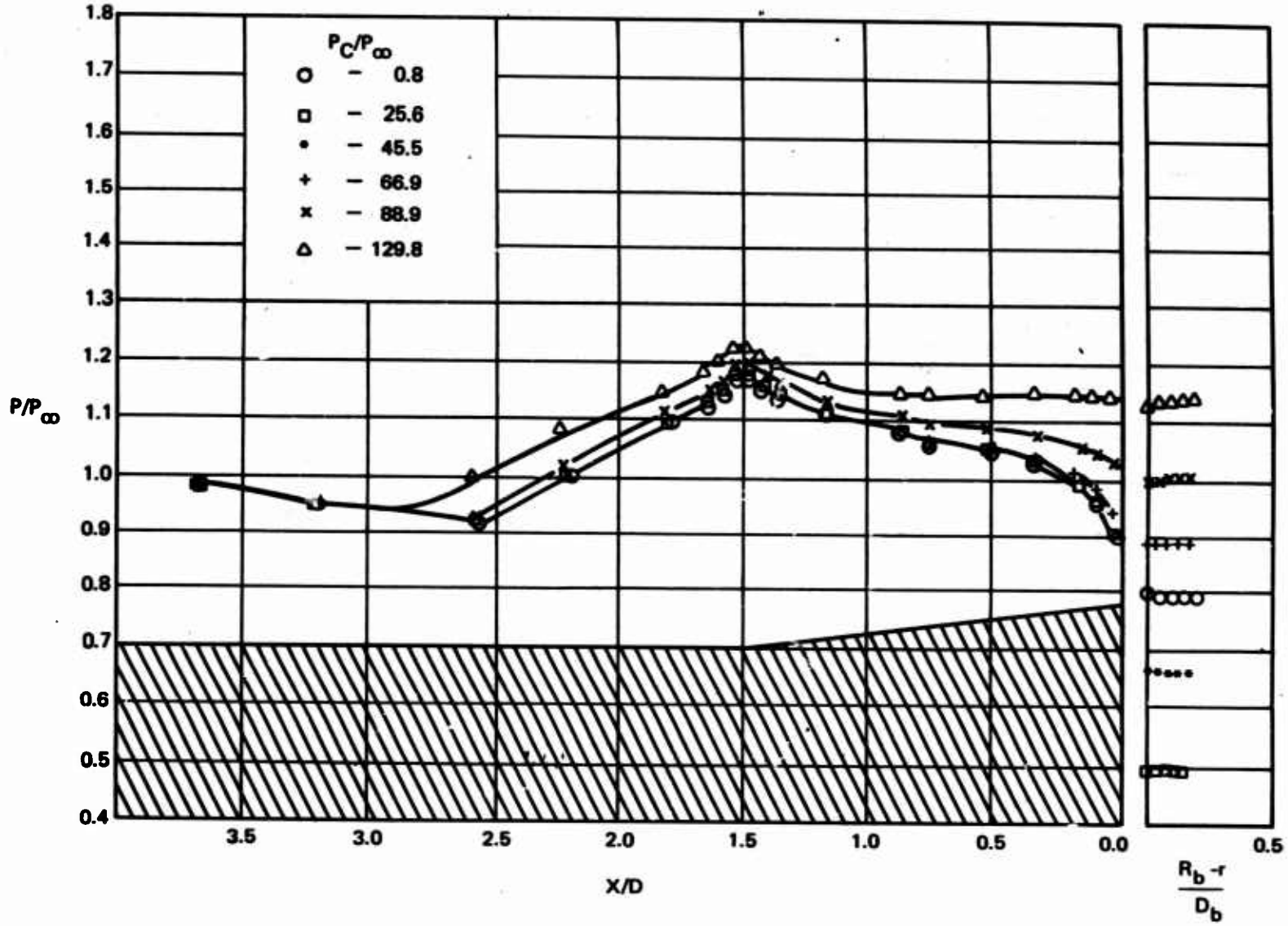

Figure 19. Flare Body Pressure Distribution Configuration B_8N_1, $M_\infty = 1.0$, $\alpha = 0$ Degree

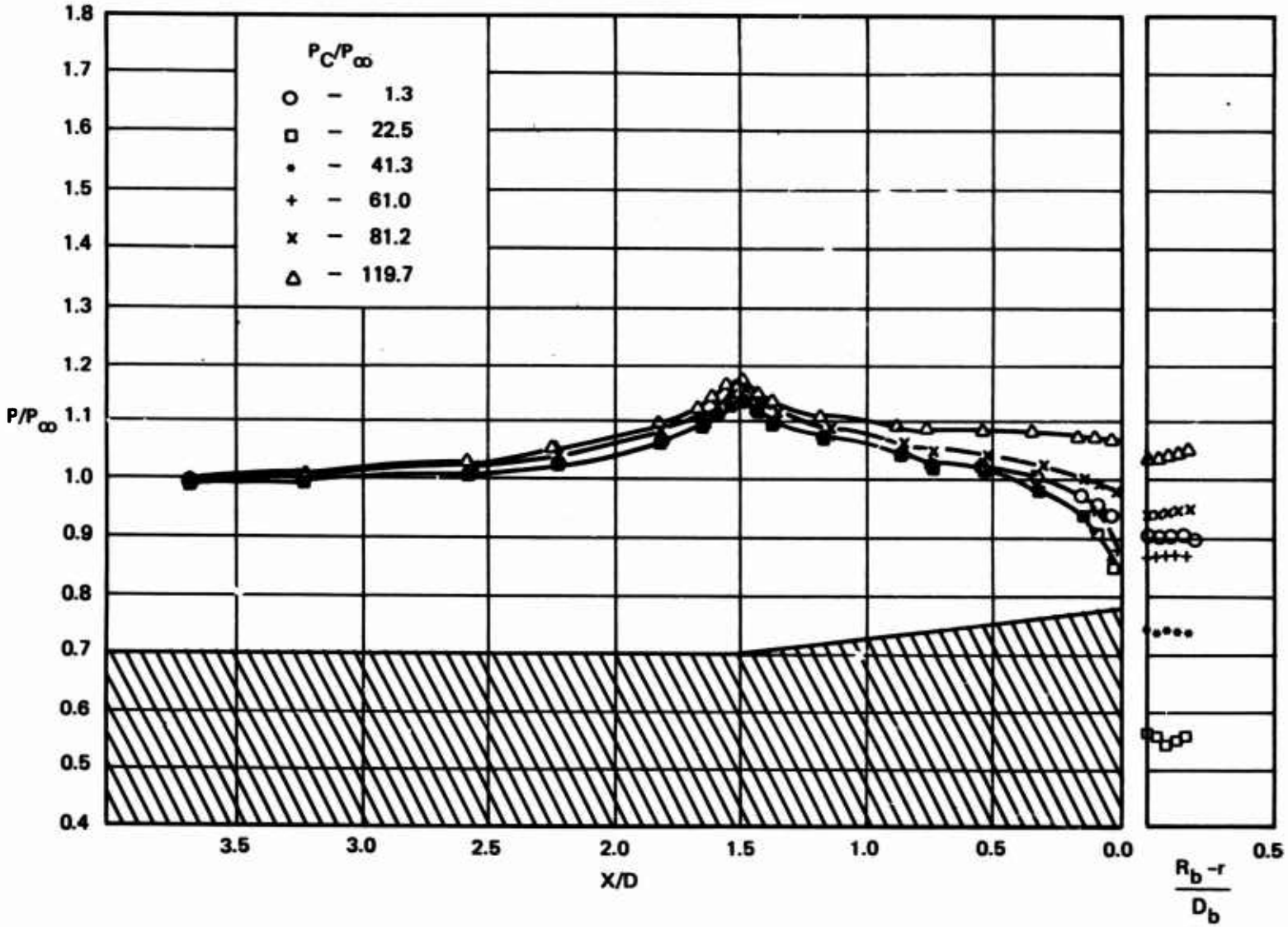

Figure 20. Flare Body Pressure Distribution Configuration B_8N_1, $M_\infty = 0.9$, $\alpha = 0$ Degree

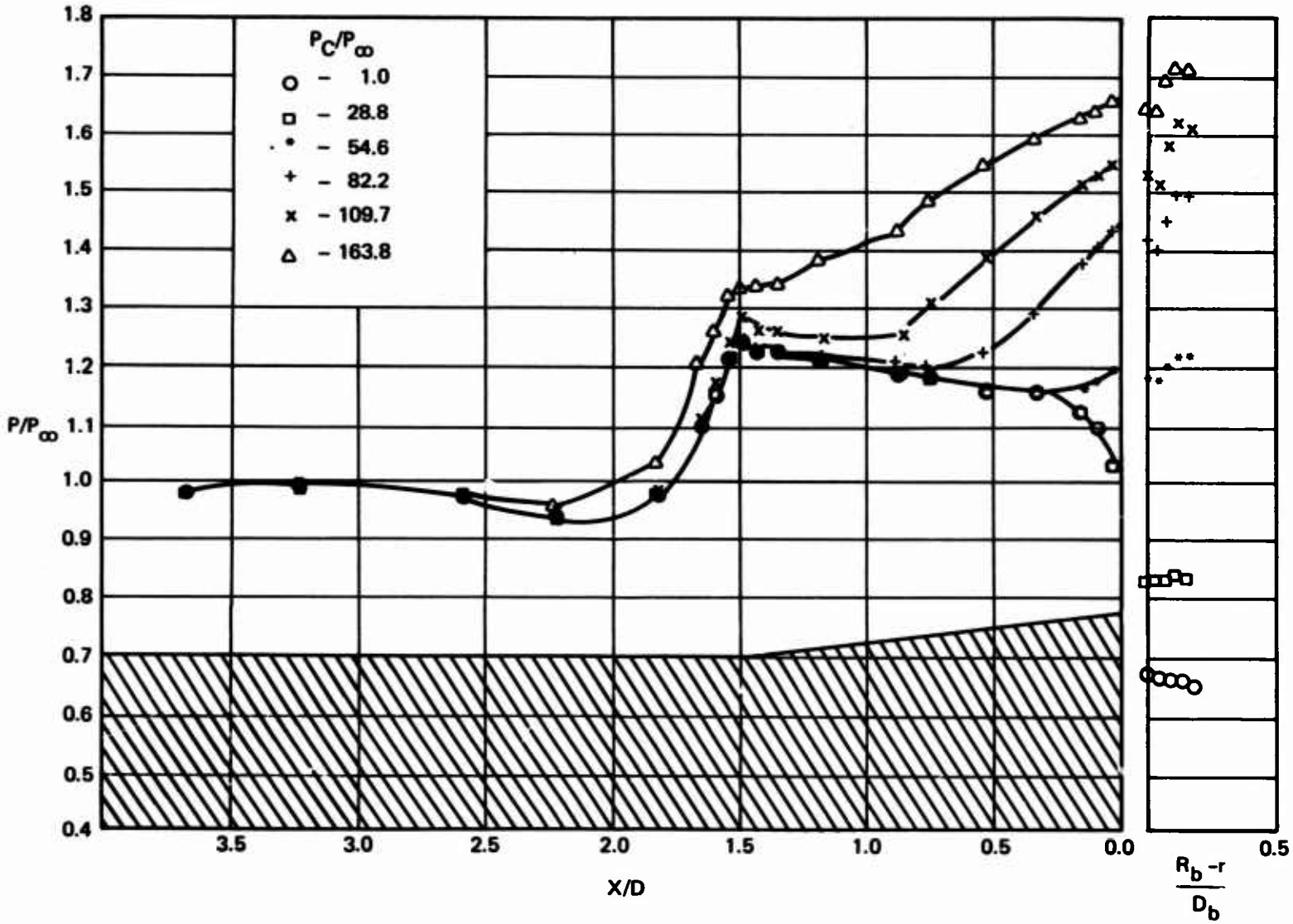

Figure 21. Flare Body Pressure Distribution Configuration B_8N_{14}, $M_\infty = 1.2$, $\alpha = 0$ Degree

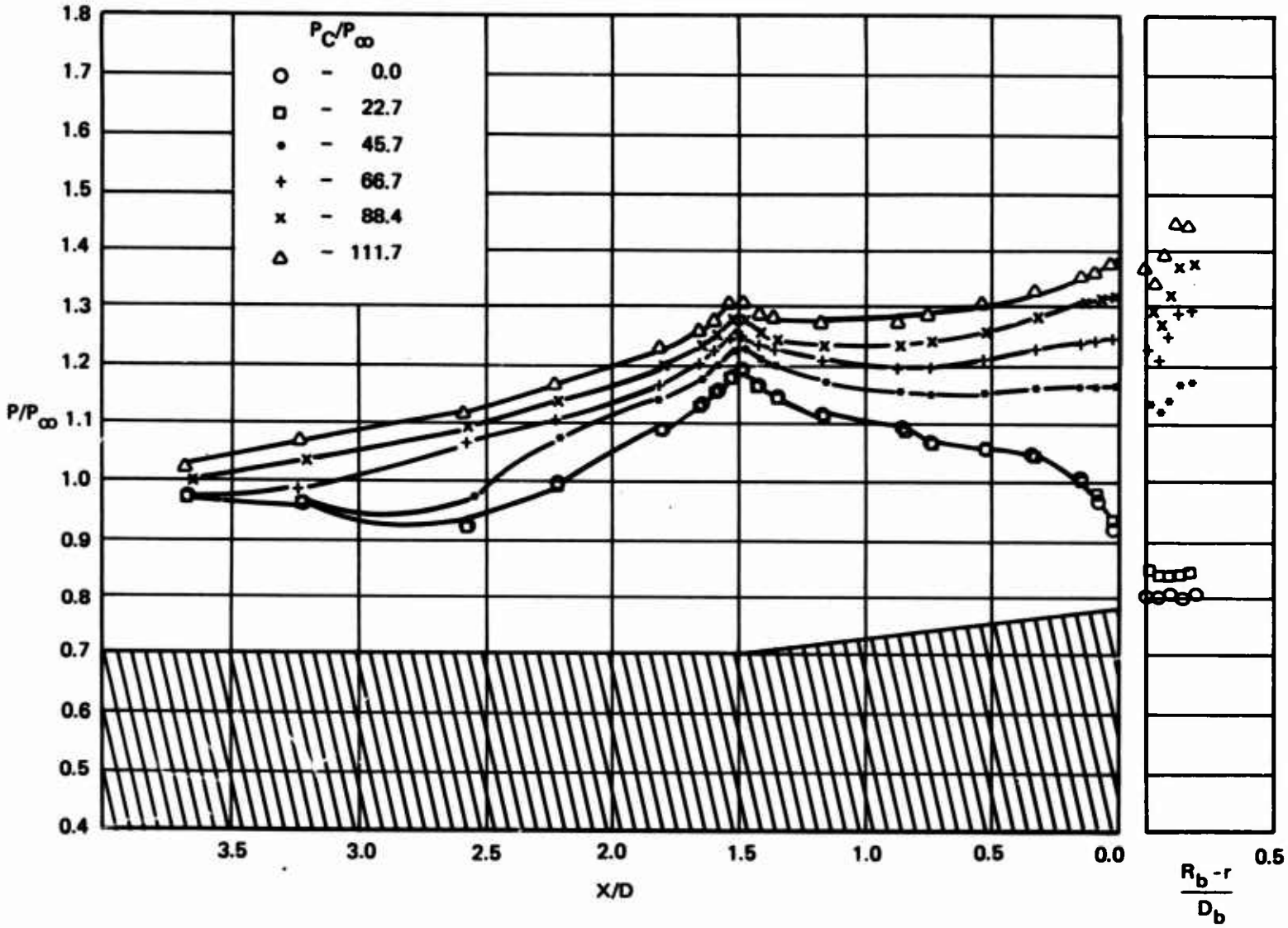

Figure 22. Flare Body Pressure Distribution Configuration B_8N_{14}, $M_\infty = 1.0$, $\alpha = 0$ Degree

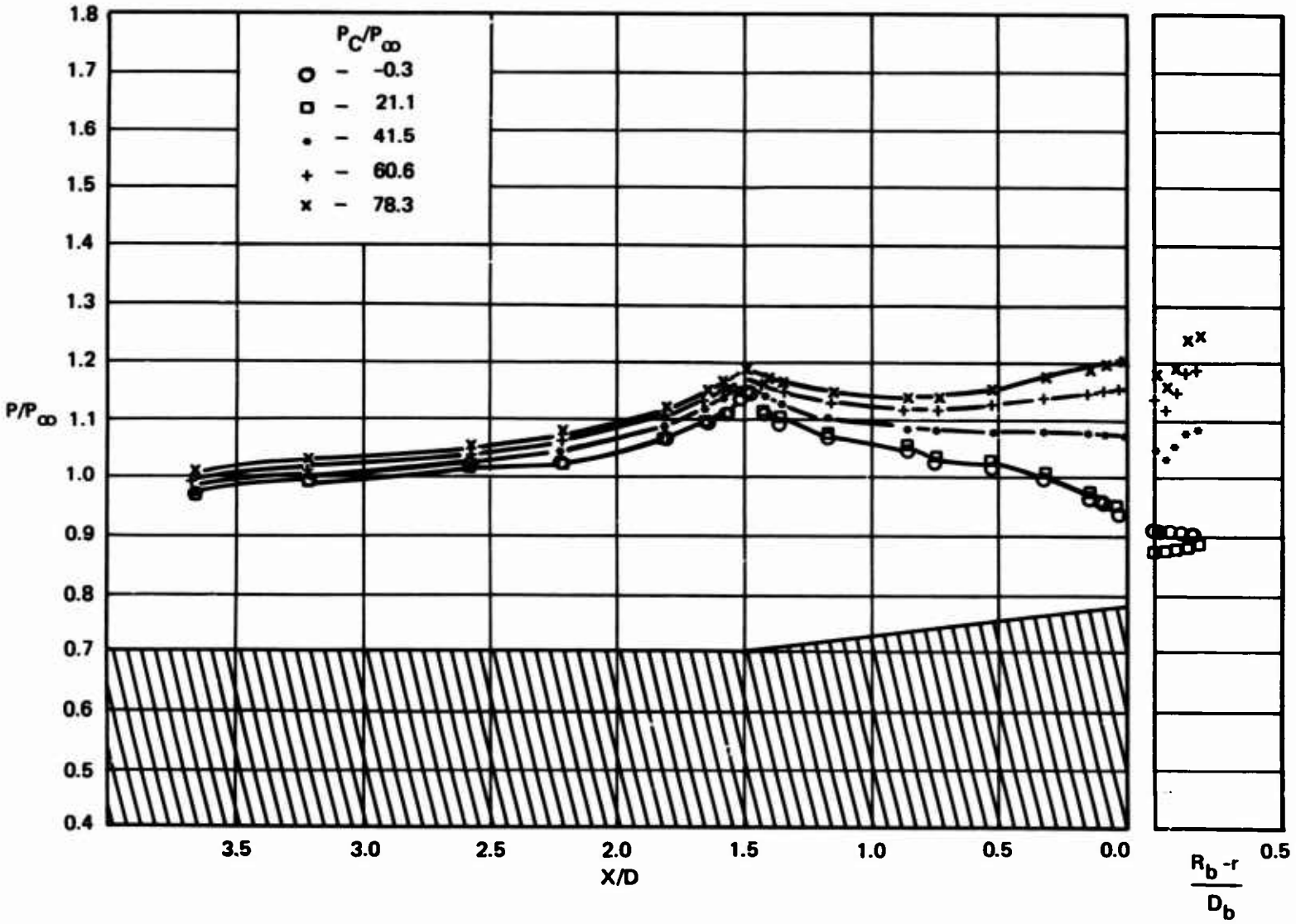

Figure 23. Flare Body Pressure Distribution Configuration B_8N_{14}, $M_\infty = 0.9$, $\alpha = 0$ Degree

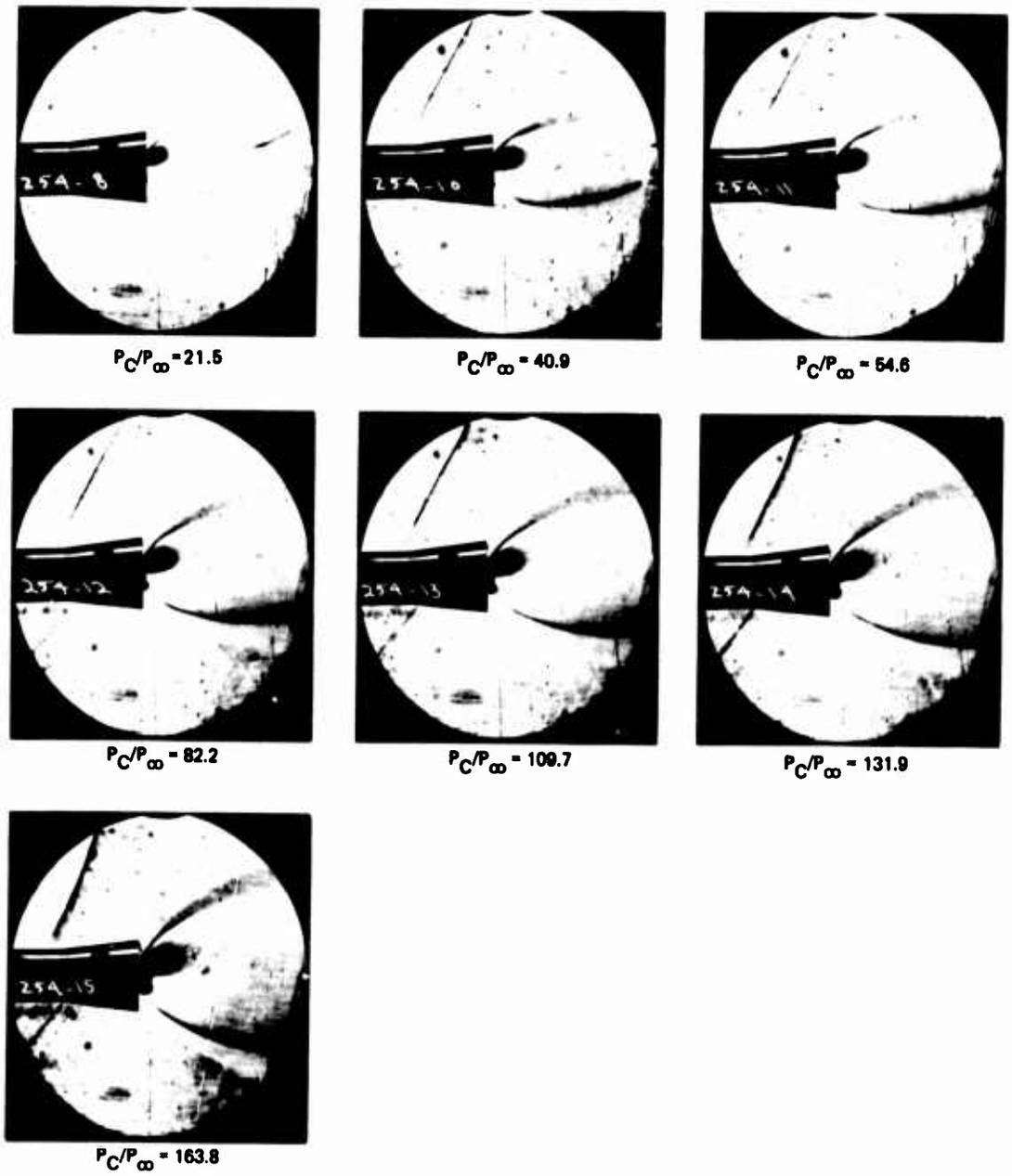

Figure 24. Schlieren Photographs Configuration B_8N_{14}, M_∞ = 1.2, α = 0 Degree

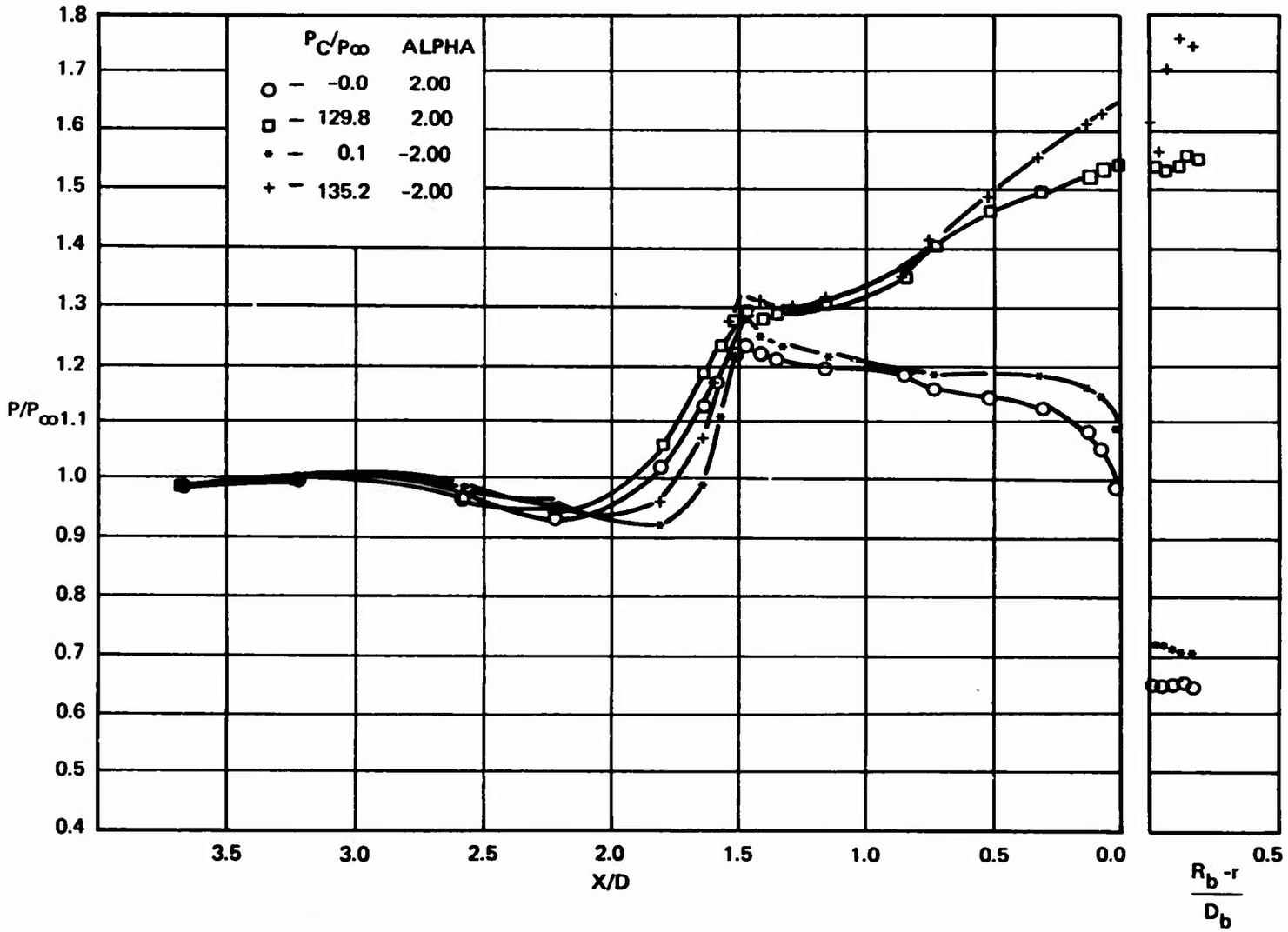

Figure 25. Flare Body Pressure Distribution at Angle of Attack Configuration B_8N_{14}, $M_\infty = 1.2$

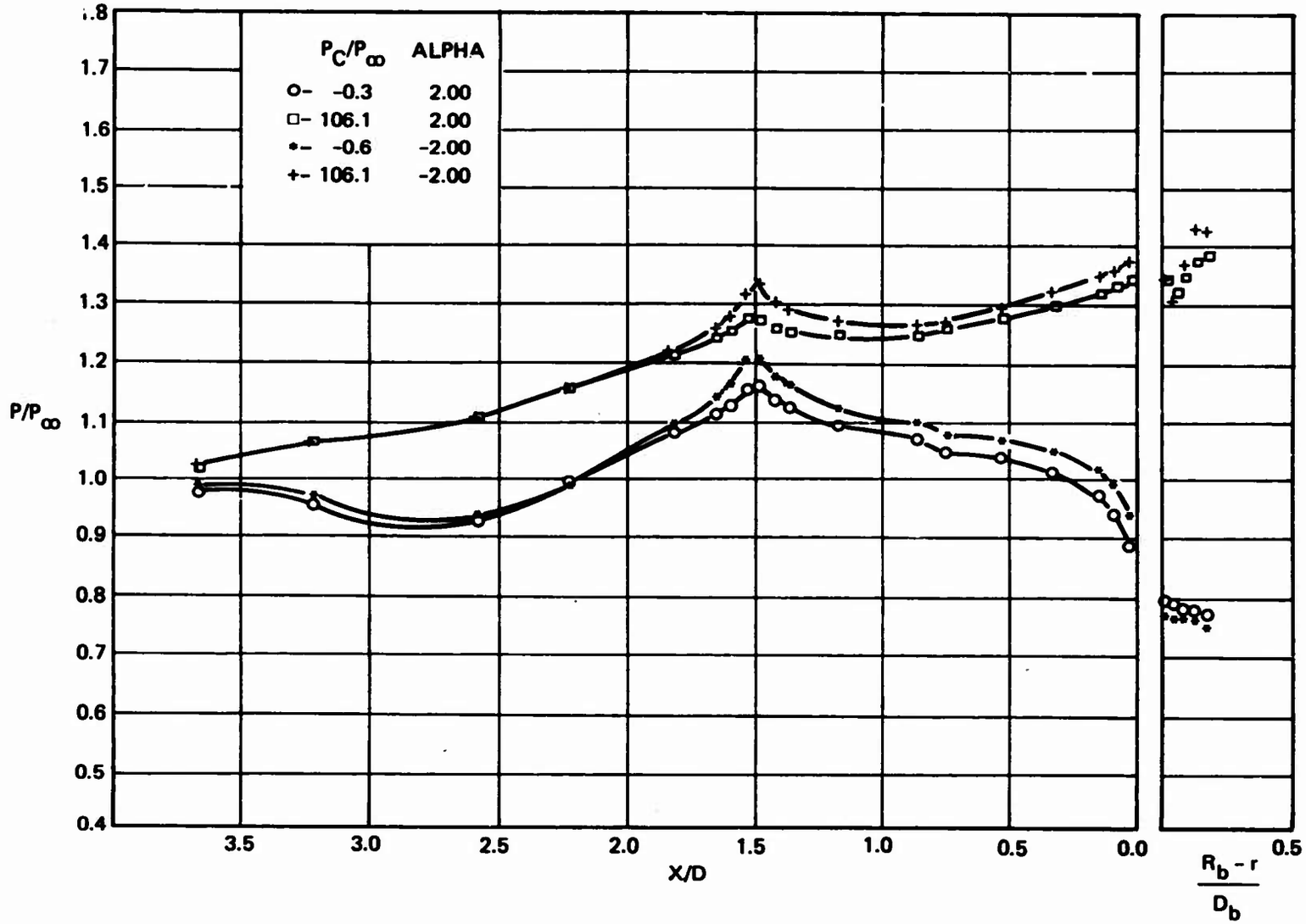

Figure 26. Flare Body Pressure Distribution at Angle of Attack Configuration B_8N_{14}, $M_\infty = 1.0$

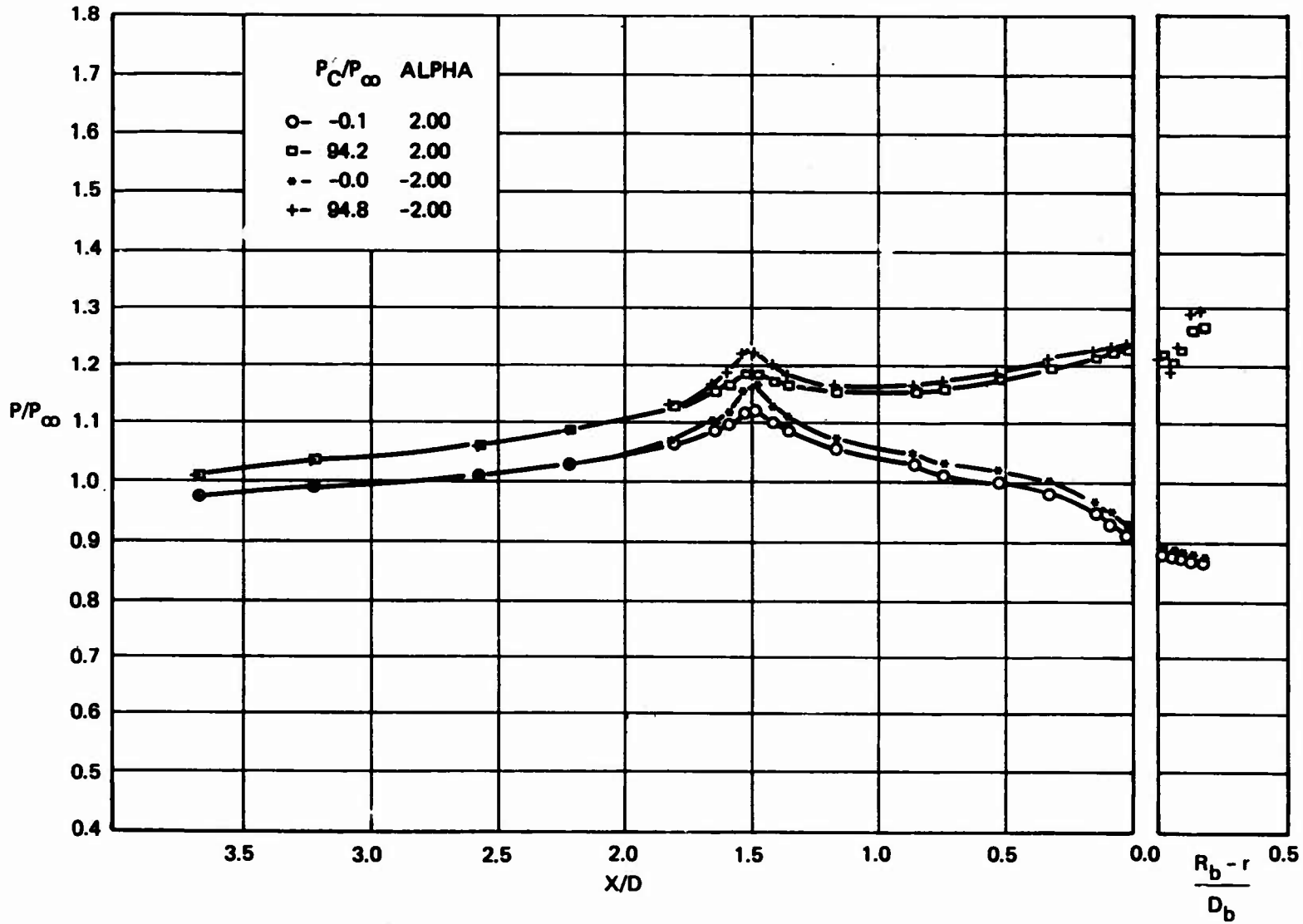

Figure 27. Flare Body Pressure Distribution at Angle of Attack Configuration B_8N_{14}, $M_\infty = 0.9$

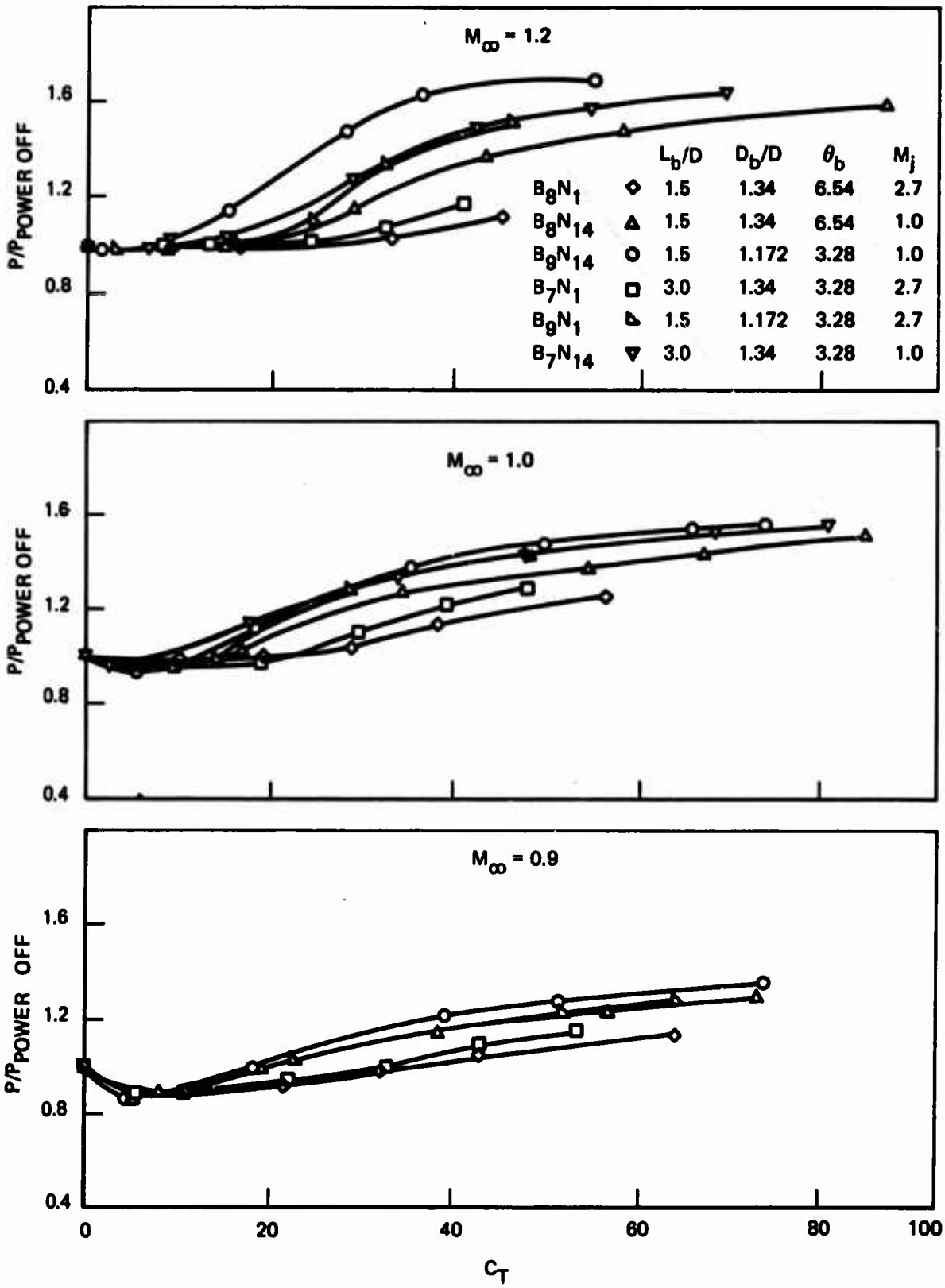

Figure 28. Flare $P/P_{Power\ Off}$ at Station X/D = 0.025 for Varying C_T

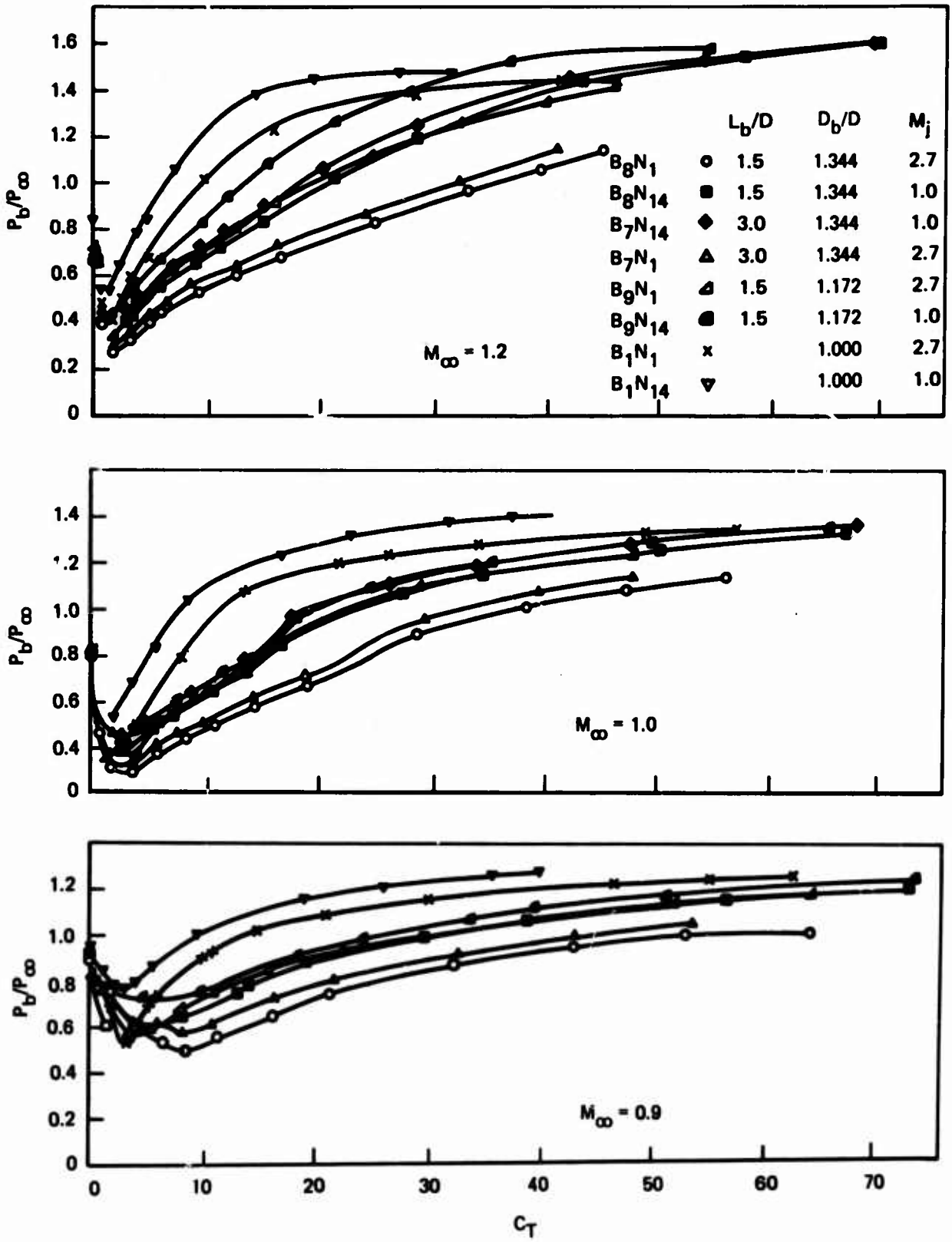

Figure 29. Flare P_b/P_∞ Versus C_T

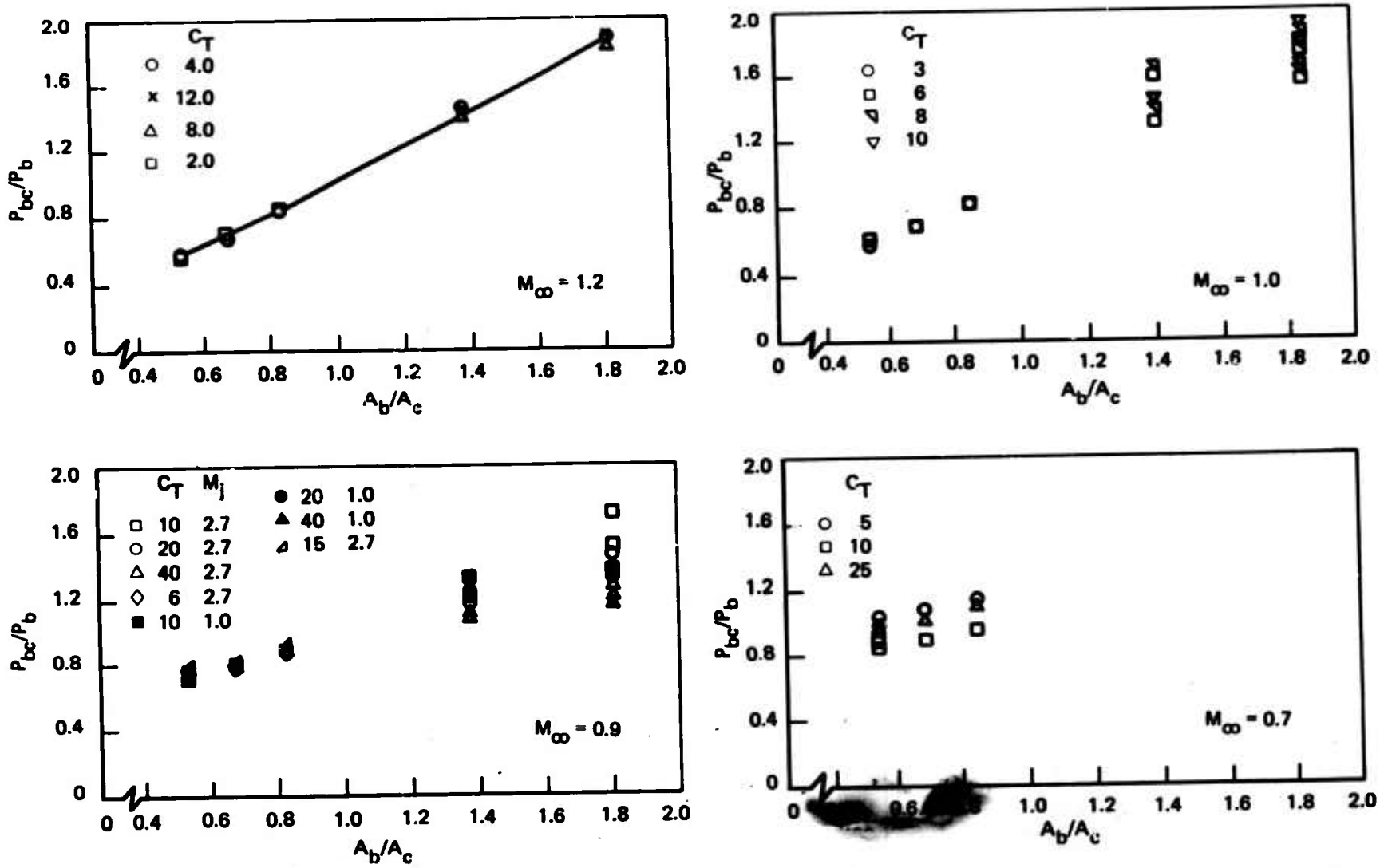

Figure 30. Proportionality Factor as a Function of Base Area Ratio